sustainability

MDPI

Article

Classification of Post-COVID-19 Emotions with Residual-Based Separable Convolution Networks and EEG Signals

Qaisar Abbas [1], Abdul Rauf Baig [1,*] and Ayyaz Hussain [2]

[1] College of Computer and Information Sciences, Imam Mohammad Ibn Saud Islamic University (IMSIU), Riyadh 11432, Saudi Arabia
[2] Department of Computer Science, Quaid-i-Azam University, Islamabad 44000, Pakistan
* Correspondence: abbaig@imamu.edu.sa; Tel.: +966-563336816

Abstract: The COVID-19 epidemic has created highly unprocessed emotions that trigger stress, anxiety, or panic attacks. These attacks exhibit physical symptoms that may easily lead to misdiagnosis. Deep-learning (DL)-based classification approaches for emotion detection based on electroencephalography (EEG) signals are computationally costly. Nowadays, limiting memory potency, considerable training, and hyperparameter optimization are always needed for DL models. As a result, they are inappropriate for real-time applications, which require large computational resources to detect anxiety and stress through EEG signals. However, a two-dimensional residual separable convolution network (RCN) architecture can considerably enhance the efficiency of parameter use and calculation time. The primary aim of this study was to detect emotions in undergraduate students who had recently experienced COVID-19 by analyzing EEG signals. A novel separable convolution model that combines residual connection (RCN-L) and light gradient boosting machine (LightGBM) techniques was developed. To evaluate the performance, this paper used different statistical metrics. The RCN-L achieved an accuracy (ACC) of 0.9263, a sensitivity (SE) of 0.9246, a specificity (SP) of 0.9282, an F1-score of 0.9264, and an area under the curve (AUC) of 0.9263 when compared to other approaches. In the proposed RCN-L system, the network avoids the tedious detection and classification process for post-COVID-19 emotions while still achieving impressive network training performance and a significant reduction in learnable parameters. This paper also concludes that the emotions of students are highly impacted by COVID-19 scenarios.

Keywords: COVID-19; stress; anxiety; internet of things; health informatics; emotion recognition; depthwise separable convolutional neural network; light gradient boosting machine

Citation: Abbas, Q.; Baig, A.R.; Hussain, A. Classification of Post-COVID-19 Emotions with Residual-Based Separable Convolution Networks and EEG Signals. *Sustainability* **2023**, *15*, 1293. https://doi.org/10.3390/su15021293

Academic Editors: Mohamed Haffar, Fiona Oster and Carlos Salavera

Received: 8 December 2022
Revised: 4 January 2023
Accepted: 6 January 2023
Published: 10 January 2023

1. Introduction

Several studies in the field of psychology suggest that emotional health is an important aspect of well-being. As a result, it is worrisome to observe that mental depression cases are on the rise across the world [1]. A considerable portion of the population in many developed and developing countries suffers from mental illnesses [2]. The emergence of the COVID-19 epidemic has made the situation worse [3]. As a result, the ratio of mental patients to psychiatrists or psychologists has increased even more. According to one estimate, 62% of Americans experience acute stress in the months following COVID-19 recovery. Anxiety is one of the more long-term symptoms of post-COVID-19 syndrome (PCS), also known as Long COVID, a relatively new diagnosis. After recovering from the condition, between 23% and 26% of people, mainly females, experience mental health issues (including anxiety). Up to 25% of people, according to a 2021 study, experienced higher anxiety for at least 3 months after recovering from COVID-19. According to a 2021 study, if you have had COVID-19 [3–5], you may have a greater risk of complications with major organ systems (kidneys, heart, lungs, and liver) after being discharged from the hospital. Furthermore, these patients are prone to cardiovascular disease (CVD). Human beings are

emotional creatures, and this is a trait that sets them apart from other living beings [6]. From relationships to decision-making, and even expressing oneself, emotions ultimately alter a person's behavior [7,8]. A build-up of unprocessed emotions is a common trigger for anxiety or panic attacks [9–12]. These attacks exhibit physical symptoms that may easily lead to misdiagnosis. These symptoms include sharp chest pains, lightheadedness, nausea, difficulty breathing, dizziness, headaches, and even stomach aches. Internet of Things (IoT) devices, sensors, and artificial intelligence (AI) make users' lives more comfortable and provide a feasible solution for healthcare applications [13]. IoT devices such as sensors are embedded into physical devices along with machine learning methods to monitor and exchange data. In practice, there are faster ways through which doctors, with the help of IoT technology, can assess a patient's emotional wellness. Global researchers from around the world have been working to develop automatic methods for tracking mental depression, particularly using EEG data. In this field, many machine learning and deep learning approaches, as well as various feature selection methods, are receiving greater attention.

Deep learning (DL) is one of the methodologies that can be used to calculate emotional factors. Several studies use DL-based classification algorithms to predict the user's mental state from EEG signal data [14]. The hardware measures the modes and frequencies of biological electro-signals gathered from brain waves. Electroencephalography (EEG) has been the most convenient brain imaging method that can reveal the brain's electrical activity in real-time applications in daily areas of life. The brain dynamics when using an EEG are highly challenging to construe, especially if the signal comprises both noise and brain dynamics [15]. Therefore, the need for signal filtration to achieve the desired electrical activity becomes important. The frequency domain of the EEG provides a view of the sequential events of processing streams in the brain. DL algorithms [16,17] offer a novel solution. Nowadays, researchers are using DL models for image or signal recognition and classification based on the Convolutional Neural Network (CNN), which is among the most successful algorithms.

Medical experts may be able to avoid some of these issues by using automated, accurate classification algorithms for EEG readings. The Depthwise Separable Convolution (DS-Conv) network presented here, which has a lower computational cost and fewer parameters than traditional heavy DL networks such as those in [18–20], replaces them without sacrificing performance, having up to 27 times fewer operations and 32 times fewer parameters than VGG-16, but with only a 0.9 percent decrease in accuracy. In image-based recognition systems, a learning-based technique known as DS-Conv has recently been successfully employed for feature extraction [16–21]. The depthwise separable CNN (DSC) models outperform when compared with traditional manual feature extraction methods and some earlier transfer learning (TL) models. In this paper, the RCN-L anxiety and stress detection method being proposed is based on residual connections and a DS-Conv depthwise separable convolution neural network with a light gradient boosting machine (LightGBM). By combining residual connection and light gradient boosting machine (LightGBM) techniques, this paper presents a novel depth-separable convolution model called RCN-L. To develop an RCN-L system, the first step is to remove artifacts and convert the 1-D EEG data into a 2-D spectrogram image through a transformation phase. Later, the feature extraction step is performed on spectrogram images through the DS-Conv method and finally classified by the LightGBM classifier.

1.1. Aim of Study

The primary aim of this study was to detect emotions in undergraduate students who have recently experienced COVID-19 through analyzing their EEG signals. In this study, we used EEG signals due to several reasons. First, as a diagnostic measure, EEG is the preferred mechanism by which anxiety, stress, and normal emotions are detected by healthcare practitioners. Second, as pointed out in the literature review, there have been numerous studies detecting emotions from EEG with DL technologies with high predictive measures. However according to the best of our knowledge, we have not found any study,

in the post-COVID-19 context, for measuring physiological disorder among undergraduate students. In addition, we compare non-COVID-19 and post-COVID-19 brain conditions of individuals to demonstrate the differences in detecting emotions using the proposed technique. As a result, the main EEG characteristics of each condition are identified, which can be potentially useful in making informed diagnosis decisions in clinical settings.

1.2. Major Contributions

The following are the important contributions of the presented method:

(1) Development of a novel RCN-L system to detect post-COVID-19 stress and anxiety symptoms among undergraduate students. The RCN-L model is less computationally expensive and requires fewer parameters.
(2) Preprocessing of the EEG signal to remove noise and convert it to a spectrogram image structure through the short-time Fourier transform (STFT).
(3) Efficient extraction of features from spectrogram images; a lightweight pre-trained CNN model which is based upon separable convolution has been developed for this purpose.
(4) Automatic classification of post-COVID-19 stress and anxiety by using a light gradient boosting machine (LightGBM), a machine learning technique.
(5) In terms of accuracy and the number of parameters, an efficient reduced-redundancy 2D separable convolution approach for diagnosis of post-COVID-19 stress and anxiety from EEG signals.

2. Literature Review

Several EEG-based state-of-the-art studies have been developed for the detection and classification of emotions using machine learning (ML) and DL algorithms. Since there is no single study on detecting the effect of post-COVID-19 on study or work performance, especially on employees' or students' mental health, many of the other state-of-the-art systems that have been developed are described in the following paragraphs.

According to the authors of the study [22], EEG data was collected using four screen-printed active electrodes that were then integrated into a headband. The signal was then analyzed in real-time using an open-source software that extracts, classifies, and visualizes brain signals. In another study [23], a database of standardized movie clips was created to target four types of emotions: surprise, sadness, disgust, and anger. The subjects were shown forty clips to use as elicitation material. For that study, fifty healthy people (25 men and 25 women) were considered. The study employed a deep learning network based on the long-term short-term memory (LSTM) model to distinguish negative and positive emotions.

In the paper [24], the authors used 32 healthy volunteers who viewed a 40-min movie of emotional music, and their EEG signals were captured via 32 electrodes located on their skulls using the DEAP dataset. The three major components of feature extraction were asymmetric, regional, and temporal feature extractors. A convolution layer with 20 neurons was then utilized as the deep learning classifier, followed by a SoftMax layer. In another paper [25], the authors collected a dataset while subjects were watching a 40-min video of music; 32 individuals had their EEG signals recorded. Following that, approximate entropy and the wavelet transform were utilized to extract EEG features. The support vector machine (SVM) and Random Forest (RF) machine learning classifiers were then used to recognize emotions. In the paper [26], the authors used face features, EEG, and galvanic skin response (GSR) for multimodal emotion status. They used EEG signals because of their probability and reliability. To develop this system, they used Inceptionresnetv2 as the base network architecture. In another study [27], the authors used EEG and peripheral physiological data to assess levels of valence, dominance, like/dislike, arousal, and familiarity in 32 participants while they watched 40 music videos for one minute each. The MobileNetV1 on the ImageNet dataset obtained an accuracy of 70.6% [28], while the GoogleNet obtained an accuracy of 69.8%.

In another paper [29], numerous studies were carried out using a variety of techniques, necessitating a thorough examination of the strategies employed for this work, as well as their feature sets and techniques. It serves as a guide for newcomers in designing an efficient emotion recognition system. The authors proposed emotion detection using electroencephalography (EEG) signals. The BiLSTM network learns spatial features and information from several brain regions and captures long-term reliance on the EEG signal. Moreover, the authors of study [30] used a deep learning (DL) model to recognize emotions by utilizing the EEG signals.

In [31], the models were combined with a variety of machine-learning approaches. These models were tested on two tasks: the first one was social anxiety disorder classification and emotion recognition, utilizing a dataset called DEAP for physiological signal emotion analysis. Five deep (CNN) convolutional neural network models were investigated to explore robust deep features [32]. In [33], the emergence of the COVID-19 epidemic had recently made the situation worse. The ratio of patients with mental depression to psychiatrists or psychologists was alarmingly low in many nations. The suitability of four neural network-based deep learning architectures that were developed to track mental depression from EEG data was investigated and compared in the study. In [34], analyzing and classifying pre-recorded EEG data was also used to achieve a quantitative depression score. Furthermore, the results obtained by using raw EEG were far superior to those obtained using EEG. As discussed in many previous works, EEG has been studied only as a useful brain imaging tool, as discussed in [35]. The key features used in previous work to determine the accuracy of EEG in emotion detection are different emotions. EGG signals are also applicable in emotion recognition since their devices are used in clinics to aid in the diagnosis of symptoms that are used as data for analysis for further medical interventions (Table 1).

Table 1. Existing EEG-based state-of-the-art studies for detection and classification of emotions.

Cited	Features	Methods	Dataset	Accuracy
[22]	Combination approach integrating CSP+SP+PSD.	MLP, LDA, SVM, and NB	GPAED	ACC: 91.75%
[23]	Authors identify different emotion states.	KNN, EMD, MLP, SVM, and LSTM	DEAP, SEED	ACC: 94.12%
[28]	No specific emotion is used.	SVM, KNN, ANN	DEAP	ACC: 91.1%
[25]	Arousal and valence.	Wavelet transform, approximate entropy, KSR, LPP, PCA	DEAP	ACC: 50–95%
[26]	Angry, disgusted, afraid, happy, natural, sad, and surprised emotions.	InceptionResnetV2 and CNN	DEAP	LUMED-2: 81.2–74.2%
[24]	Arousal and valence.	RACNN inspired by CNN	DEAP	ACC: 96.65%
[30]	EEG signal emotion detection utilizing a feature extractor based on Linear Formulation of Differential Entropy (LF-DfE) and a BiLSTM network classifier.	Linear Formulation of Differential Entropy (LF-DfE) feature extractor and BiLSTM network	SEED and DEAP	NA
[31]	Detect the social anxiety disorder classification.	SVM and KNN	DEAP	NA
[32]	An effective deep-feature extraction-based method for automatically classifying people's emotional states. CWT to convert the EEG signals into EEG rhythm images.	Five pretrained CNN models such as MobilNetv2, VGG16, SqueezeNet, AlexNet, and ResNet50. Finally, they used SVM to classify into emotions.	DEAP	ACC: 91.07%
[33]	To examine and compare the appropriateness of emotions.	LSTM, SVM, and LR algorithms are applied on EEG data.	EEG Brainwave	ACC: 97.50%
[34]	A hybrid convolutional and temporal-convolutional neural network (CNN-TCN).	CNN-TCN	PRIVATE dataset	Mean squared error (MSE) 5.64 ± 1.6

Cmmon Spatial Pattern (CSP), Signal Power (SP), Power Spectral Destiny (PSD), univariate statistics, oscillation, Ganeva Affective Picture Database (GPAED), Multilayer Perceptron (MLP), Linear Discriminant Analysis (LDA), SVM, and Naïve Bayes (NB) classifiers, Regional-Asymmetric Convolutional Neural Network (RACNN), hybrid convolutional and temporal-convolutional neural network (CNN-TCN).

3. Materials and Methods

3.1. Data Acquisition

The EEG data were captured using the ThinkGear AM (TGAM) board and quantified in the frequency bands using the power delta (0.3–5 Hz), theta (4–11 Hz), alpha (12–16 Hz), and gamma (17–28 Hz). In the case study, an EEG signal data set (PostCovid-EEG) was used to verify the effectiveness of the suggested RCN-L methodology. There were extensive comparisons with existing EEG classification techniques. The Covid-EEG dataset contained different male and female subjects with different age groups. In fact, this dataset was collected based on the 30-min recording of EEG signals during the practice of five algebraic mathematical questions. This study engaged the participation of around 120 participants. The study's participants were all undergraduate engineering students. With ages ranging from 20 to 26, there were 20 female students and 100 male students (20 with anxiety, 20 with stress, and 80 with normal states). The dataset was uneven, and this may have created bias issues. To handle this issue, this research employed 10-fold cross validation to remove the biases from the model. All participants were investigated for normal, stress, and anxiety emotions' concerns after getting COVID-19. In general, the data was collected after a minimum of 30 days of COVID-19. These participants were already on medication and were under psychological treatment. They were selected at random, with the only condition being that they were in their first or second semester at university. All assessments were administered at the end of the semester to alleviate students' anxiety about their academic responsibilities and/or exams.

It should be emphasized that the ThinkGear AM (TGAM) headset is a non-invasive brain–computer interface (BCI) device made for gathering unprocessed EEG data from the human brain for scientific study. The output signals have a frequency range of 0.2 Hz to 45 Hz, with a notch at 50 Hz for noise reduction caused by the AC power source. The subjects' body movements, muscular movements, and eye blinking are kept to a minimum throughout the data collection. Artifacts such as visual, motion, sensory, and electrical artifacts can have a significant impact on the categorization method's effectiveness. Therefore, it is crucial to introduce the artifact removal approach. Prior to being sent to the feature extraction phase, the EEG signals obtained from the sensors are first pre-processed to remove these artifacts. The denoising technique was used in this paper to divide the signals into sub-bands using the discrete wavelet transform (DWT).

3.2. Proposed Methodology

The primary goal of this paper was to confirm that emotion is impacted by post-COVID-19 scenarios. As indicated in the systematic diagram in Figure 1, the proposed system combined residual connection and light gradient boosting machine (RCN-L) based on four primary phases. In the first phase, the multi-channel EEG signals are preprocessed to remove artifacts, and these 1-D EEG signals are converted into a 2-D spectrogram image. In the second phase, the depthwise and pointwise separable CNN (DSC-Conv) models with the residual network are utilized to extract relevant features. The unique DS-Conv-based classifier is then given these features, which creates probabilities for every output class in different time blocks. In the fourth phase, the LightGBM handling step integrates probabilities from several time blocks to boost detection confidence. To extract features from spectrogram images, the DSC and residual connection-based CNN models are used first. The images are then classified using LightGBM classifier into stress and anxiety. The next subsections will explain each of these phases in more detail.

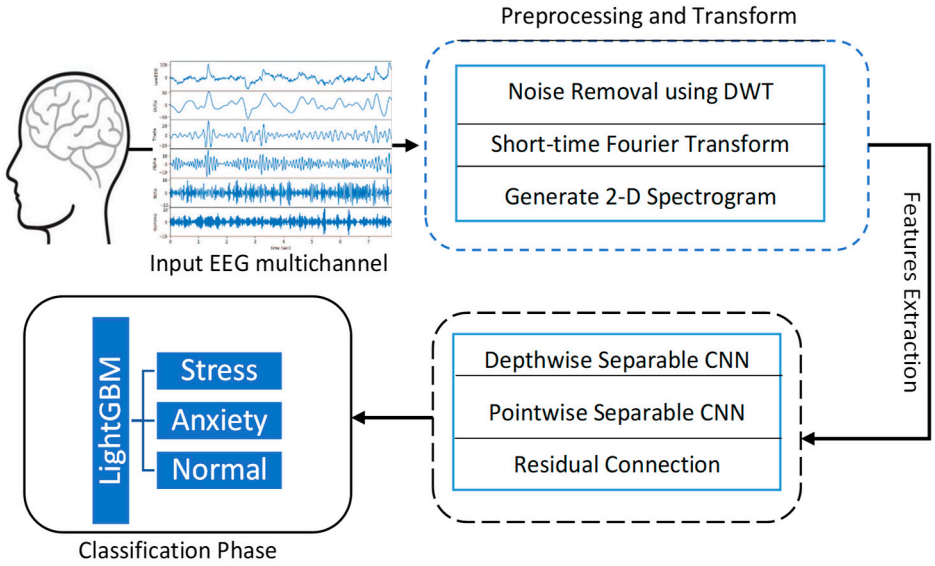

Figure 1. The proposed architecture based on a residual connection with a depthwise and pointwise separable convolution neural network (DSC-Conv) that extracts features and then classifies them using a LightGBM machine learning algorithm.

3.2.1. Preprocessing and Signal Transformation

The EEG data were captured using the ThinkGear AM (TGAM) board and quantified in the frequency bands using the power delta (0.3–5 Hz), theta (4–11 Hz), alpha (12–16 Hz), and gamma (17–28 Hz). These multichannel EEG signals are recorded on human scalps, and they are invariably noisy (due to EEG artefacts and small interference). EEG signals are first subjected [36] to a denoising technique to expose their features. A wavelet threshold denoising method was utilized in this paper as described in study [36]. The Daubechies wavelet of order 6 (dB6) was selected as the mother wavelet for denoising using the discrete wavelet transform (DWT). Based on experiments, this paper selected dB6 over the entire Daubechies wavelet family to obtain the optimal wavelet. This work used a DWT noise removal method to remove eye blink or muscular distortions from EEG recordings. In de-noising physiological signals, wavelet de-noising outperforms signal frequency domain filtering because it preserves signal properties while reducing noise. Denoised EEG data can be used to analyze information from different emotional states, particularly stress and anxiety. After removing artifacts, the next step was to convert preprocessed 1-D multi-channel signals into 2-D spectrogram images by using the short-time Fourier transform (STFT) method.

The fast Fourier transform (FFT) is an algorithm that allows calculating the discrete Fourier transform, widely used in the process analysis of signals [37]. The FFT estimates the magnitude and phase of the sinusoidal components' periodicals, allowing one to reconstruct a signal as the linear combination of these components, which allows one to describe a signal in the frequency domain and in an analysis of time-dependent components. The fast Fourier transform (FFT) is a method to extract features and is used for extracting the finer emotional details such as spectral entropy and spectral centroid. The FFT extracts these simple features from the alpha, beta, and alpha to gamma frequencies. Given that theta and delta have extremely low frequencies, the lower frequencies are not needed for their lack of sufficient information in the FFT method. After the signal has been filtered and only the relevant signals are available, these signals are unidentified and need to be classified. The k-nearest neighbors (KNN) algorithm has a majority voting scheme, which is used to classify unidentified signals. The new data are given a classification with the highest number of votes. The majority vote schemes are used instead of similarity vote schemes because they are less sensitive to the outliers, which aids the FFT since it is a method for extracting the finer details [20]. In fact, recent research has demonstrated that

multiple fundamental frequency estimation performs exceptionally well in the magnitude spectrogram domain. As a result, we have applied spectrogram images to classify brain signals into stress, anxiety, and normal conditions.

The short-time Fourier transform (STFT) for non-stationary signals [38–43] is generally used (Equation (1)) even where a signal is divided into small segments and the smoothed FFT is calculated as a window for each segment, to avoid the effects generated by the truncations from the series; it is assumed that the signal has stationary features in short segments of time. When the frequencies vary wildly in the different parts of the program, no matter the size of the window, you could lose information. The inconvenience is that the analysis is made with a single resolution. In these cases, it is convenient to use Wavelets functions.

$$STFT(t_0, f) = \sum^{\infty} x(n)v(n - t_0)e^{-2\pi jfn} \quad (1)$$

The parameters of Equation (1) are as follows: $x(n)$ is an input signal, $v(n)$ is the window size, t_0 is the window clearance, f is frequency, and n is the number of current samples. Note that the window size effect is a small window (good time, bad time) and a big window (suitcase in time, good in frequency). According to Equation (1), the value of t_0 moves to the center of the window and the FFT is estimated for that segment that has a width the same as that of the window. This allows estimating the evolution of the spectrum by moving the window throughout the signal by adjusting the t_0 parameter. In addition, this process results in a three-dimensional graph that represents the energy of the frequency content of the signals and that varies over time. Finally, the energy of the signal can be estimated to elevate the STFT to the square (see Equation (2)).

$$Spectrogram = \| \sum_{-\infty}^{\infty} x(n)v(n - t_0)e^{-2\pi jfn} \Big\|^2 \quad (2)$$

where the spectrogram image is constructed and $x(n)$ is an input signal, $v(n)$ is the window size, $t0$ is the window offset, the f parameter represents frequency, and n is the number of current samples. A visual example of signal preprocessing and transforming 1-D EEG signals into a 2-D image spectrogram is displayed in Figure 2. Also, a spectrogram is a representation between three dimensions (temporal, frequency, and amplitude) of the energy distribution of a signal; an example of a spectrogram can be seen in Figure 3.

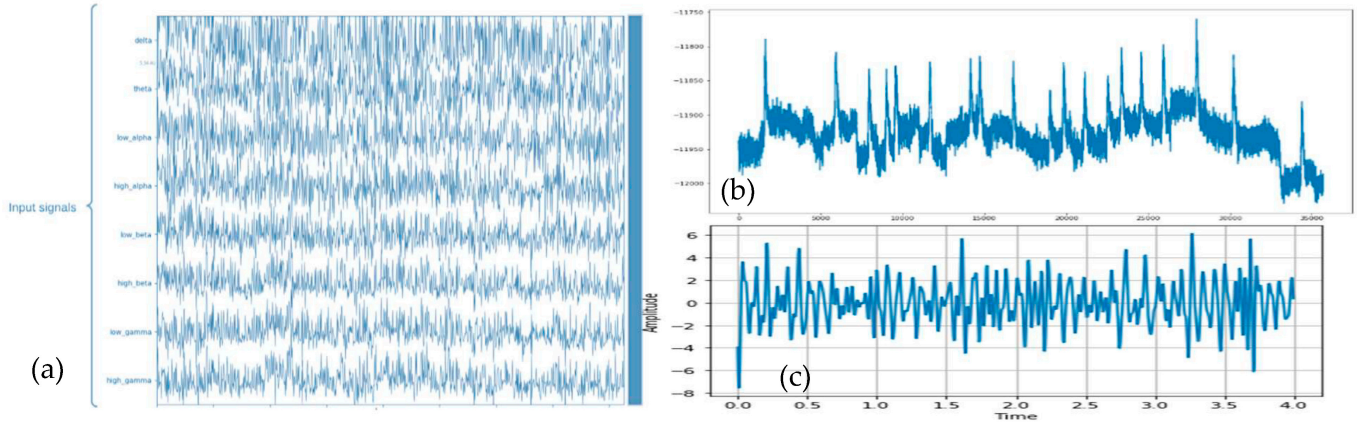

Figure 2. *Cont.*

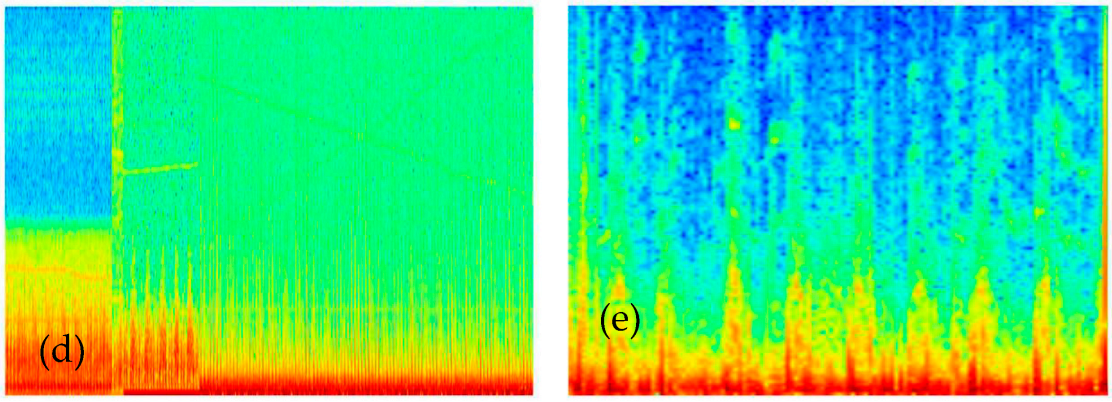

Figure 2. Visual example of signal preprocessing and transforming 1-D EEG signals into 2-D image spectrogram, where figure (**a**) shows the input multichannel signals, (**b**) represents the theta signal segment, (**c**) shows the zoom-in of figure (**b**), and figure (**d**,**e**) shows the transforming of 1-D into 2-D spectrogram images.

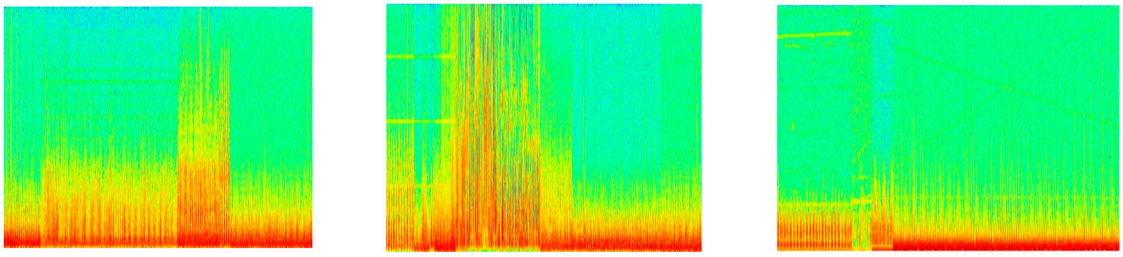

(**a**) (**b**) (**c**)

Figure 3. An example of anxiety spectrogram for (**a**) stress, (**b**) anxiety, and (**c**) normal states.

3.2.2. Augmentation to Control Imbalance Data

The application of data augmentation techniques is carried out to control imbalance data. As a result, it is difficult to find a more appropriate and efficient augmentation method for designing the multi-label diagnosis system. Data augmentation operations often involve flipping, rotating, reflecting, shifting, zooming, contrasting, coloring, and noise disruption [29–31].

To create the RCN-L model, all spectrogram pictures in the collected dataset were normalized from [0, 255] to [−1,1]. The CNN model requires a huge dataset to attain high-performance accuracy. Furthermore, due to an over-fitting issue, the CNN architecture's performance deteriorated with a short dataset, implying that the model performs well on training data yet underperforms on test data. The data augmentation method was used in this research to enlarge the dataset to alleviate the problem of over-fitting. As a result, the dataset size can be enhanced using simple image processing methods as well as the data augmentation approach. The augmentation method is shown in Table 2 and visually displayed in Figure 4, including the parameters.

Table 2. Data augmentation with defined parameters.

Method	Parameters
Rotation-range	20
Width_shift-range	0.1
Shear-range	0.3
Zoom-range	0.3
Horizontal-flip	True
Vertical-flip	False

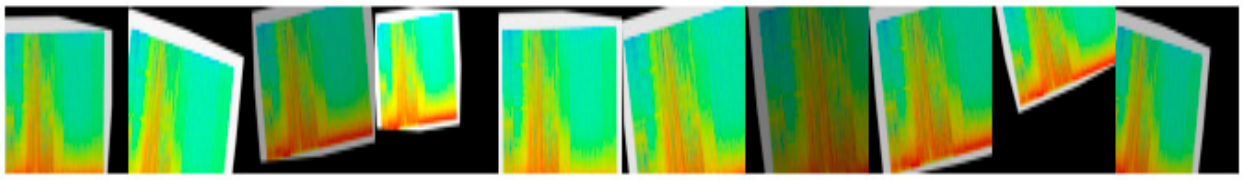

Figure 4. Data augmentation technique applied to anxiety spectrogram image.

3.2.3. Features Extraction by RCN-L Classifier

A newly proposed RCN-L system was provided to detect and classify human emotions into stress and anxiety with post-COVID-19 conditions. To develop this RCN-L system, two convolutional layers with a kernel size of (3 × 3), three residual blocks (b1, b2, b3) with two depthwise and pointwise convolutional layers and one pointwise convolution (PC1) layer, three Max Pooling layers (MP1, MP2, MP3), four batch normalization (BN) layers, and one convolution layer with a kernel size of 1 were used to build the feature map in this design. One projection convolution layer, one expansion layer, and one sequence and excitation block were also included in the network design. After that, one dense layer, one flat layer, one global averaging pooling layer, and finally, a LightGBM classifier with linear activation function, were used for classification. The systematic flow diagram is displayed in Figure 5. In addition, Algorithm 1 displays all the steps used to develop an effective feature extraction strategy and those phases are explained in the subsequent paragraphs.

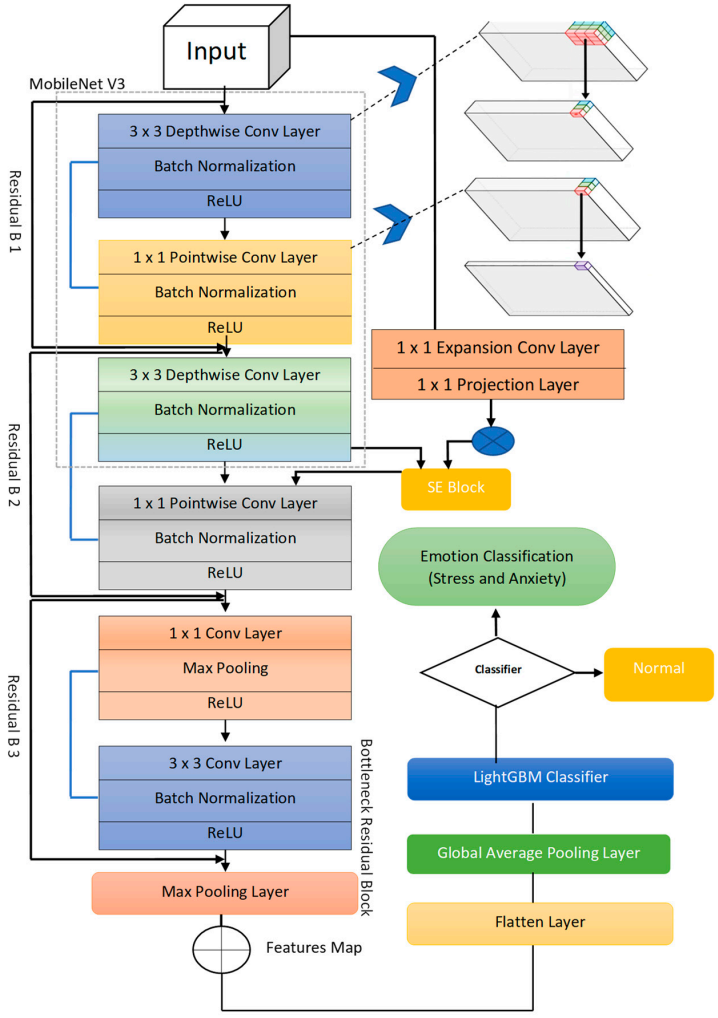

Figure 5. A systematic flow diagram of proposed RCN-L deep learning, which is based on depthwise convolution and pointwise convolution along with Light-GBM classifier.

For depthwise convolutional layers, the kernel size was set to (3 × 3), with a boundary of 2 and a stride of 2. The pooling layers likewise employed a kernel size of (3 × 3) and a stride of 2. Batch normalization, which was applied right after each separable convolution layer before the activation function, may improve the efficiency and stability of deep neural network training. In addition, the Rectifier linear unit exponential linear units (RELU) function was used to define the output value of kernel weights and convolutional layers for each depthwise and pointwise convolutional layer. This adds a tiny amount of information to the classification process. Further, the flatten layer was used to flatten the feature, the dense layer was used to minimize the size of the feature, and the LightGBM classifier was used to classify the spectrogram image of the features into normal, stress, and anxiety.

EEG spectrogram signals are very complicated when there are EEG features to be extracted. As a result, the MobileNetV3 model was utilized as a backbone to extract and learn the most informative features from spectrogram images by using deep learning (DL) architecture. In practice, the MobileNetV3 block includes a fundamental building block called the residual block, which includes a depthwise separable convolution block and a squeeze-and-excitation (SE) block. The SE block is employed to pay more attention to the relevant features on each channel during training without sacrificing computational time. The MobileNetV3 was developed by Howard et al. in 2019.

MobileNetV3 is based on depthwise separable convolutions and was introduced for mobile and embedded vision applications in [44]. MobileNet [45] is a lightweight deep convolutional neural network class that is much smaller and runs much faster than many other popular models. Depthwise separate convolutions apply a single filter to each input to filter the data, then merge these filters together into a set of output features using 1 × 1 convolutions. These depthwise separable layers perform almost identically to traditional convolution layers but at a significantly faster pace and with a minor change. To implement minor change in the architecture, we have added a depthwise separable convolution, the normal convolution filters, and merge them into output features. This is divided into two layers, one for filtering and another for mixing. This reduces the size of the model and the amount of computing power required. Except for the final fully connected layer, which feeds into a softmax layer for classification with no nonlinearity, all layers are followed by batch norm and ReLU nonlinearity. Without counting depthwise and pointwise convolutions, MobileNet comprises different layers. The batch normalization layer and the rectified linear unit are added at the end of each convolutional layer. The MobileNetV3 has an inverted residual process for making linear bottlenecks with the increase in feature maps from 24 maps to 144 maps and the reduction in feature maps from 144 maps to 24 maps. Mobile Net's architecture aids in depthwise separable convolutions, replacing computationally demanding convolutional layers, which are critical in computer vision applications [46]. The depthwise separable CNN (DSC) offers two advantages for constructing a deep learning model: (1) it can help minimize parameters, and (2) it can be used to improve model generalization. As a result, it is safe to say that DSC improves detection accuracy and training effectiveness.

Algorithm 1: Proposed depthwise and pointwise separable network

Input: Input Tensor (X), signals representation in form of spectogram.
Output: Extracted and generate feature map $x = (x_1, x_2, \ldots\ldots, x_n)$ from preprocessed 2-D spectrogram image
Main Process:
Step 1. Depthwise and pointwise CNN blocks
Step 2. Repeat for Each block
(a) Depthwise-CNN is applied to tensor x by kernel size of (3 × 3), which includes a number of filters, branch normalization, ReLU activation function is applied.
(b) Pointwise-CNN is applied to tensor x by kernel size of (1 × 1), which includes a number of filters, branch normalization, ReLU activation function is applied.
[End Step 2]

Algorithm 1: Cont.

Step 3: Squeeze and Excitation (SE) block contains expansion (1 × 1), Projection (1 × 1) layers
Step 4. Model Construction
(a) (3 × 3) of two Conv layers, each with 32 and 64 filters, ReLU() function.
(b) Three skip-connections are applied to the network and each one skip includes two separable layers followed by maxpooling. The skip connection has Conv of 1 × 1 with strides 2.
Step 5. Afterward, the feature map $x = (x_1, x_2, \ldots\ldots, x_n)$ generated by using flatten layer.

Depthwise separable CNN (DSC) was first introduced in the field of image classification by a few studies [47]. DSC has been used in a variety of real-time applications in many studies. The conventional convolution is factorized into depthwise and pointwise convolutions via DSC. The single convolution filtering per channel is performed by depthwise convolution, which is followed by pointwise convolution, which is a linear combination of the depthwise convolutional output. The following is a formula for depthwise convolution:

$$Depthwise_{conv(w,y)_{i,j}} = \sum_{K,L}^{k,L} W_{k,l}.\, y(i+k, j+l) \tag{3}$$

The following is a formula for pointwise convolution:

$$Pointwise_{conv(w,y)_{i,j}} = \sum_{m}^{M} W_m.y(i,j,m) \tag{4}$$

DSC is an exceptional convolution class that combines pointwise convolution with depthwise convolution using a 1 × 1 kernel. When compared to regular convolution, DSC is specifically developed to reduce the computational complexity and learnable parameters. It was demonstrated that, when compared to the traditional convolution approach, 3 × 3 DSC might reduce the overall number of trainable parameters by eight to nine times. DSC achieves the same result by dividing the kernels into two and doing fewer multiplications. Each channel is considered separately, with one filter per channel being convolutional over that channel. Each input channel must be convolutional with a single precise kernel using the standard convolution method. By using a higher kernel size, you can reduce your processing costs even more. The DSC was developed as an alternative to the usual convolution structure in the present work to reduce the number of calculating operations while retaining CNN network generalization, as illustrated in Figure 4. The DSC model divides the calculation of convolution into two stages: (1) for filtering, each channel is convoluted utilizing depthwise convolution; (2) for combining, pointwise convolution is convolutional kernel. A pointwise convolution is then used to connect the depthwise convolution outputs. A criterion convolution is used to make a new output set that filters out and merges the input in one step.

As demonstrated in Figure 5, a deep neural network model was created by using MobileNetV3 as a backbone architecture. In general, the model used 1 × 1 convolution to minimize the dimension of the input spectrogram data cube, extracting a lot of spectral information. There are three residual units, R1, R2, and R3, which were then used to extract both spatial contextual and spectral aspects of the data cube indefinitely. Finally, instead of using the fully connected layer, a combination of 1 × 1 convolution and global average pooling (GAP) layer merged extracted abstract features and provided the most informative features for final signal classification task. Furthermore, this paper has presented per layer network architectural steps in Figure 4. First, the network was fed with processed spectrogram data in the shape of 11 × 11 × 200 (200 being the number of bands). The first layer, C1, which has 38 of the 1 × 1 kernels, reconstructs channel properties from the raw input data while retaining spatial information. The R1 block, which consists of two 3 × 3 kernels with stride = 1, was then used to preserve spatial edge information. After the

R1 block, the very first layer of R2 was a 3 × 3 filter with stride = 2 for down sampling, and the second layer was a 3 × 3 kernel with step size of 1 for generating 6 × 6 × 70 feature tensors.

The depthwise and pointwise separable CNN isolates channels by extracting only their input channels' features rather than combining them to form new ones. Each channel requires a pointwise convolutional layer to improve channel correlation and recreate new input features. The architecture is made up of two depthwise and two pointwise convolutions that allow for substantially faster evaluation than classical convolution. For faster learning performance, a batch-normalization layer with the rectified linear unit (ReLU) activation function is used after the convolutional layer. Due to the rapid increase in training time and expense, large kernel sizes are no longer employed. Weights are regularly altered to choose the incoming data's valid spatial information. ReLU was chosen as the activation function to introduce non-linearity into the network. Finally, every network produces a probability feature vector that forecasts the probability of each output class.

$$Costfunction,\ L(\theta) = L_{DSC}(f(a), b) + \frac{\lambda}{2m} \times \sum \|w\|^2 \tag{5}$$

The loss function $L_{DSC}(f(a), b)$ is used to calibrate the compatibility between both the desired output and network predictions. Weight matrices value reduction reduces network overfitting and facilitates model generalization due to the use of L2 regularization. The λ parameter shows the regularization parameter, and θ represents the set of filters, biases, and ReLU parameters to be estimated.

3.3. Transfer Learning

The goal of transfer learning (TL) [32] is to provide a study area in DL to apply information gained, while addressing one issue to another that is comparable. Instance-based, parameterized, feature-representation, and relational knowledge transfer learning methods may be generally divided into four categories. The strategy that seeks to find effective feature representations that can be applied across domains, feature-representation transfer learning, is the most appropriate among these groups. In the suggested method, domain-independent image characteristics are extracted using pre-trained CNNs, which increases the transferability from source to target domain. The classification head is utilized instead of the top layers in a CNN that has already been trained on ImageNet. Pre-trained models are chosen wherever possible since the training time has been dramatically reduced. TL is primarily used to reduce training overhead. The pre-trained models combine feature extraction and fine-tuning to create new ones. We can adjust by adding additional layers to support the new classes. Here, we apply the fine-tuning approach. A pre-trained model is extended using the fine-tuning method to fit the requirements of the new dataset. The model does not need to be completely trained from the beginning. This shortens the training period. A few additional layers will be trained in this case by adjusting the weights while training. The weights will be adjusted during training to better match the characteristics of our dataset. The convolutional networks' upper layers are often more specialized. The lowest layers pick up simple, universal properties that apply to many photos. The characteristics become more tailored to the dataset being used to train the model as they go up the network. Instead of replacing general learning, the primary objective of fine-tuning is to employ the specialized features with the required dataset. Fine-tuning can help to improve performance.

We demonstrated the suggested methodology using the MobileNetV3 network as a pretrained backbone architecture for effective features extraction. The initial weights were loaded into the basic models when they were created. The network was then trained using the fully connected model, which was added to this loaded model. The following sections go into great depth about each model's specifics. To prevent overfitting, we simply made the last convolutional block more precise rather than the entire network. It makes sense to keep the first few blocks unchanged (more general features) and only fine-tune the last block since low-level convolutional blocks learn characteristics that are less abstract and

more generic than those discovered from higher layers (more specialized features). To guarantee that the changes remain extremely small and do not influence the previously learned characteristics, fine-tuning is carried out at a very modest learning rate. The effectiveness of the network capacity decreases when more levels are frozen. As a result, we only learned the final classifier at the beginning, after freezing all the layers. Then, to have a better outcome, we thought about gradually unfreezing more layers, starting at the top. Networks that have been trained on a small amount of data may overfit the training set.

The weights utilized in the training of the original model were used as the beginning weights for the MobilenetV2 [37] model. A dropout layer comes after the global average pooling layer. If overfitting is dealt with, increasing the network's depth can enhance outcomes. Overfitting is avoided by using L2 regularization. The original model's training weight from ImageNet was utilized to establish the weight. We utilized the binary cross-entropy logarithmic loss function because there are only two class variables.

3.4. Features Classification by LightGBM

The LightGBM classifier is used to recognize classes of emotions because of its efficiency in dealing with very small datasets, including its performance in high-dimensional domains, and this paper picked the LightGBM classifier for this investigation. They also have a three-class classification challenge, which is why they used LightGBM. LightGBM [47,48], and XgBoost have detection performance that is comparable to or greater than Random Forest. When the detection efficiency of LightGBM and XgBoost is compared, LightGBM training and testing times are much less than those of XgBoost. The Gradient Boosting Decision Tree (GBDT) algorithm has been improved with LightGBM. It merges the predictions of several decision trees to provide a final prediction that is highly generalizable. The overall steps for the LightGBM classifier are shown in Algorithm 2.

Algorithm 2: Light Gradient Decision Boosting Machine (LightGBM)

Input: Extracted Feature Data with labels y = 0,1 and Test Data
Output: Class Labels (Stress, Anxiety, Normal)
Process:
Step 1. First, initialize tree as a constant: $y_i^t = f_0 = 0$ for optimization and parameter defined for the classifier.
Step 2. Construct LightGBM tree by minimizing the lost function:

$$f_t(x_i) = \text{argmin } L(t) = \text{argminL } (y,\ y + f\ (x)) \tag{6}$$

(a) The LightGBM () classifier is perfectly trained on the feature samples that are extracted by separable CNN along with three residual blocks.
(b) Get the next model in an additive manner:

$$y_i^t = y_i^t + f(x) \tag{7}$$

Step 3 Repeat Step 2 until the model reaches stop condition.
Step 4. Test samples y_i^t are assigned the class label using the decision function of the below equation

$$y_i^t = \sum_{t=0}^{M-1} f_t(x_i) \tag{8}$$

The main concept of the LightGBM classifier is to combine numerous "weak" learners into a "strong" one. There are two main reasons why machine learning methods based on this concept should be designed. To begin with, "weak" learners are easily obtainable. Second, combining many learners often outperforms a single learner in terms of generalization. Several recent studies have shown that LightGBM outperforms other machine learning algorithms in a variety of tasks, including air quality prediction [49] and tumor categorization [50,51]. For the most part, the features are mutually exclusive in a sparse feature space, so those features can securely bundle into a single feature. Therefore, the features create histograms from feature bundles in the same way that it is done from individual features.

The complexity of histograms is therefore increased. This paper used it because the training time is greatly sped up without sacrificing accuracy. Another benefit of LightGBM is that it allows for the best possible division of category features. As a result, LightGBM may deal directly with data category attributes. On the other hand, many other machine learning methods do not support the category features processing and must first do the numerical translation (such as label encoding or one-hot encoding). This transformation converts the data into a format that machine learning algorithms can understand, but the data becomes sparse as a result. By using a grouping strategy, LightGBM allows for the best possible split of category features. This avoids the sparse data created by the numerical translation in this approach. The LightGBM typically has a lower number of decision trees and fewer leaves per decision tree in the final model. LightGBM saves time in the decision-making phase because of this model feature. The LightGBM is a tree-based technique that supports categorical features, making feature numerical translation and normalization unnecessary during the data preprocessing phase. In the decision-making step, the leaf-wise tree growth technique makes the matching efficient. Because of these benefits, we consider LightGBM to be very effective and have adopted it as the categorization system for stress, anxiety, and normal conditions following COVID-19.

4. Results

4.1. Performance Assessment

Metrics were used to assess both existing and proposed solutions. *Accuracy (ACC)* was the initial measurement used in the experiments. This statistic was employed to assess the performance of classification models. In other words, it served as a technique for gauging how effectively the algorithm classifies the data. Additionally, improving the quality of the model reduced the potentially significant cost of mistakes. It may also be computed using the formula below:

$$Accuracy\ (ACC) = \frac{TP + TN}{TP + TN + FP + FN} \times 100 \tag{9}$$

The algorithms' ability to forecast whether a piece of data was real or false was shown by the terms "true positive" (*TP*) and "true negative" (*TN*). False Positive (*FP*) and False Negative (*FN*) indicators indicated that the algorithm mis-predicted the data, whether it was true or false. Sensitivity (SEN), the second metric, was the percentage of cases that were positive but were essentially anticipated to be positive. It shows the percentage of good incidents that were mistakenly categorized as negative. It is important to note that this measurement suggests that a high recall rate nearly invariably goes hand in hand with a low FN rate. Recall, True Positive Rate, and Hit Rate are further names for sensitivity. To calculate it, we used the formula below:

$$Senstivity(SE) = Recall\ (RL) = \frac{TP}{TP + FN} \times 100 \tag{10}$$

The third metric was *specificity (SP)*. It is characterized as the ratio of genuine negatives to all negative data in the sample. The following is the calculation for this measurement:

$$Specificity\ (SP) = \frac{TN}{TN + FP} \times 100 \tag{11}$$

The fourth metric was precision. The ratio of all successfully predicted positive categories to all accurately expected positive categories serves as a measure of the capacity to correctly identify positive categories among whole expected positive classes. The following mathematical representation is possible:

$$Precision\ (PR) = \frac{TP}{TP + FP} \times 100 \tag{12}$$

The F1-score was the fifth metric. This statistic is crucial for assessing a classifier's accuracy and resilience. The F1-score is a crucial performance measurement that takes into account both recall and accuracy. Additionally, the following calculation may be made:

$$F1 - Score = 2 \times \frac{precision \times recall}{precision + recall} \tag{13}$$

The cumulative gain curve evaluated the performance of the model by comparing the results of a random pick with the model. The graph shows the percentage of targets reached while considering a certain percentage of the population with the highest probability of being targets according to the model. Cumulative Gains for a given number of records n is the total number of true positive records among the top-n ranked records:

$$CumGain\ (n) = \sum_{j=1}^{n} y(j) = TP_n \tag{14}$$

We can also show cumulative gains as a percentage of the total possible gains (TP + FNTP + FN):

$$p - CumGains(n/N) = \frac{CumGains(n)}{TP + FN} = \frac{\sum_{j=1}^{n} y(j)}{\sum_{i=1}^{n} y(i)} = \frac{TPn}{TP + FN} \tag{15}$$

4.2. Environment Setup

To analyze the effectiveness of the proposed DS-LightGBM method, which is based on a deep learning model, the different datasets were constructed based on different training and testing ratios at various times. The whole dataset in the experiments was split into a training set and a testing set at a 3:1 ratio, meaning that three-quarters of the data was used for training and the rest was used for testing. The spectrogram image datasets were generated through the STFT approach. The proposed machine learning model was built with TensorFlow 2.9.1 and the Keras framework, and it was trained on a Tesla T4 GPU via the Google Colab platform. The Adam optimizer was used with a learning rate of 0.001, 400 epochs, a learning rate of 1×10^{-3}, and a batch size of 32 to generate the separable convolutional model. The suggested network hyperparameters are described in Table 3. In addition, this paper used seven tuned hyperparameters for the LightGBM classifier, such as leaves, feature bins, iterations, samples per leaf, model depth, learning rate, and training data.

Table 3. The proposed RCN-L network's hyperparameter settings.

Hyperparameters for RCN Classifier:						
Tensor Flow	GPU	Learning Rate	Optimizer	No of Epochs	Batch	Validation
2.9.1	Tesla T4	1×10^{-3}	Adam	400	32	10-fold
Hyperparameters for LightGBM Classifier:						
Seven hyperparameters: num_leaves: 70, max_bin: 300, n_estimators: 100, min_child_samples: 40, max_depth: 10, learning_rate: 6, and bagging-fraction: 0.8.						

GPU: Graphical Processing Unit.

4.3. Computational Cost

On the basis of computational complexity, we also compared the proposed DSC-LightGBM system with state-of-the-art models. As stated in Table 4, the suggested work required a total processing time of approximately 164.5 milliseconds (ms). The VGG-16 and Alex-Net took 184s and 209s to process in total, respectively. We used the default hyperparameters for all pre-trained models. Based on the findings, it was inferred that the suggested approach took less time to detect anxiety and stress through spectrogram

images, which is required in a real-time processing environment. In comparison to the present models, this indicates the effectiveness of the suggested concept.

Table 4. Average processing time on an EEG dataset with a recording period of 30 min.

Method	Preprocessing	Feature Extraction	Training	Prediction	Overall
Proposed	1.6 ms	1.8 ms	160.5 ms	1.4 ms	164.5 ms

milliseconds (ms).

The depthwise and pointwise separable structures have been shown to be better than ordinary convolutional layers at detecting stress and anxiety in spectrogram images and can improve network detection performance. As a result, the proposed technique outperformed the competition on various segment datasets. This separable network was also helpful in lowering the parameter size. The number of parameters in the convolutional layer of VGG-16, Alex-Net, and the separable-based CNN are compared in Table 5. The proposed model drastically reduced the number of parameters on the convolutional layer, according to the results. The findings of the experiment showed that reducing parameters did not result in degenerate models, but rather increased network generalization. In summary, the proposed RCN-L has a 30% faster running speed than some other traditional models, resulting in exceptional performance, especially with large samples, and thus laying the groundwork for its use in real-time EEG analysis systems.

Table 5. The number of parameters in the existing models' convolutional layer and the proposed model's convolutional layer RCN-L.

Layers			Parameters		
VGG-16	**Alex-Net**	**Proposed**	**VGG-16**	**Alex-Net**	**Proposed**
Conv-32	Conv-96	Conv-32	$(3 \times 3 \times 3 + 1) \times 32$	$(11 \times 11 \times 3 + 1) \times 96$	$(3 \times 3 \times 3 + 1) \times 32$
Conv-32	Conv-128	Conv-64	$(3 \times 3 \times 32 + 1) \times 32$	$(5 \times 5 \times 96 + 1) \times 128$	$(3 \times 3 \times 32 + 1) \times 64$
Conv-64	Conv-192	SConv-128	$(3 \times 3 \times 32 + 1) \times 64$	$(3 \times 3 \times 128 + 1) \times 192$	$(3 \times 3 \times 64) + (1 \times 1 \times 64 + 1) \times 128$
Conv-64	Conv-192	SConv-128	$(3 \times 3 \times 64 + 1) \times 64$	$(3 \times 3 \times 192 + 1) \times 192$	$(3 \times 3 \times 128) + (1 \times 1 \times 128 + 1) \times 128$
Conv-128	Comv-128	SConv-256	$(3 \times 3 \times 64 + 1) \times 128$	$(3 \times 3 \times 192 + 1) \times 128$	$(3 \times 3 \times 128) + (1 \times 1 \times 128 + 1) \times 256$
Conv-128		SConv-256	$(3 \times 3 \times 128 + 1) \times 128$		$(3 \times 3 \times 256) + (1 \times 1 \times 256 + 1) \times 256$
Conv-256		SConv-728	$(3 \times 3 \times 128 + 1) \times 256$		$(3 \times 3 \times 256) + (1 \times 1 \times 256 + 1) \times 728$
Conv-256		SConv-728	$(3 \times 3 \times 256 + 1) \times 256$		$(3 \times 3 \times 728) + (1 \times 1 \times 728 + 1) \times 728$
Conv-256			$(3 \times 3 \times 256 + 1) \times 256$		
Conv-256			$(3 \times 3 \times 256 + 1) \times 256$		
Conv-256			$(3 \times 3 \times 256 + 1) \times 256$		
Conv-256			$(3 \times 3 \times 256 + 1) \times 256$		
Total			3,532,576	1,191,168	87,488

4.4. Results Analysis

We created four sets of tests to demonstrate the efficacy, robustness, and generalizability of the suggested deep learning (DL) strategy for the classification of stress and anxiety in post-COVID-19 participants with various test/split ratios. The first series of trials showed how tension, anxiety, and a typical image are represented visually. The second set of experiments compared the proposed detection method to current work to better assess its performance in comparison to other systems. Figure 6 shows the effectiveness of the suggested feature extractor by comparing a few feature responses of stress and anxiety spectrogram images. In the upper part of Figure 6, the single image on the left side is the actual image, along with its features. The anxiety is not obvious in the upper image compared to the anxiety spectrogram below it. However, it can clearly detect the stress and anxiety texture information in 2D spectrogram images. As can be seen, the suggested feature extractor can extract essential texture data from both stress and anxiety images, allowing us to distinguish between them. The feature descriptor can extract significant information from spectrogram images, such as residuals.

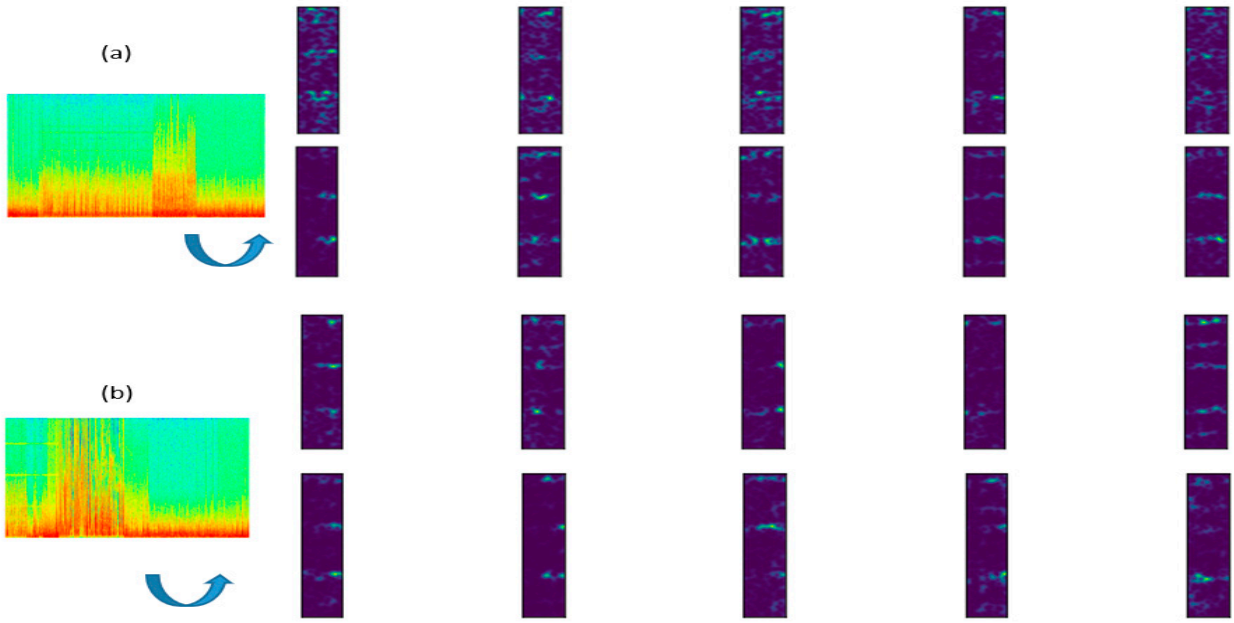

Figure 6. (**a**) Using an anxiety emotion image to represent some features of this model's last layer. (**b**) Using a stress emotion image to represent some features of this model's last layer.

Using the collected dataset, we first analyzed the proposed RCN-L model's training and validation accuracy, as well as training and validation loss functions. Figure 7 shows that the proposed model performs well, with training and validation accuracy of nearly 95% using only 400 epochs of varying lengths of recording. In addition, for training and validation data, this paper achieved a low loss function of less than 0.1, demonstrating the efficiency of the proposed approach. To evaluate the performance of the proposed RCN-L model, different segments were used to generate spectrogram images such as 8 m, 12 m, 16 m, and 22 m data, where m is shown in minutes. Compared to all other spectrogram segments, the best 12m and 16m segments were selected for performing comparisons with others because they provided better performance during the validation process, as shown in Figure 8. The proposed RCN-L model performed flawlessly on the entire dataset, as shown in the image below.

In addition, the proposed DSC-LightGBM model using the cumulative gain curve is visually displayed in Figure 9 on post-COVID-19 EEG dataset based on epochs (50, 100, 150, 200, 250, 300, 350, 400). Where the class 0 displays anxiety and class 1 represents stress emotion. This result demonstrated that the proposed classifier is outperformed in recognition of both emotion classes.

The proposed model had 92 percent accuracy and a 0.256 percent loss function on both training and validation data after 400 epochs. This was because, when utilizing the DSC-Conv model with LightGBM, it may extract more informative features that can help us improve detection accuracy. This paper concluded that using DSC-Conv and bearing this in mind together on an EEG spectrogram image is much more effective. There is a need to use the confusion matrix to fully measure the detection performance. The confusion matrices revealed that the expected and actual labels were not in concordance. The genuine label for each row was presented on the row labels, while the predicted label for every column was displayed on the column labels. The color indicated the proportion of records in the same row as the total number of entries. Therefore, based on the test set classified by the RCN-L model, we were able to acquire the results of two categories, such as anxiety and stress.

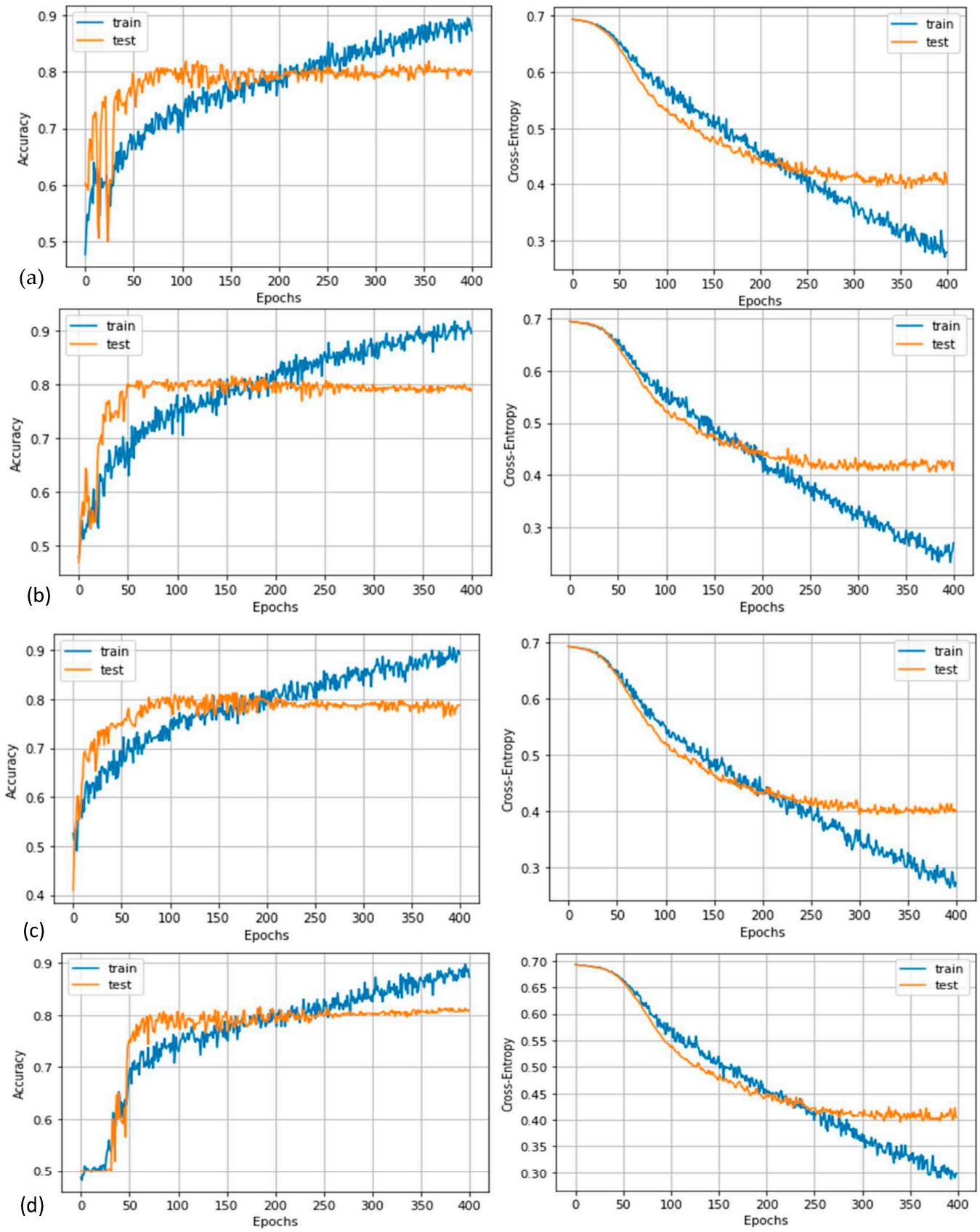

Figure 7. Training and validation accuracy and loss using PostCovid-EEG dataset in different time slots, where figures (**a**–**d**) are calculated based on 8 m, 12 m, 16 m, and 22 m, respectively.

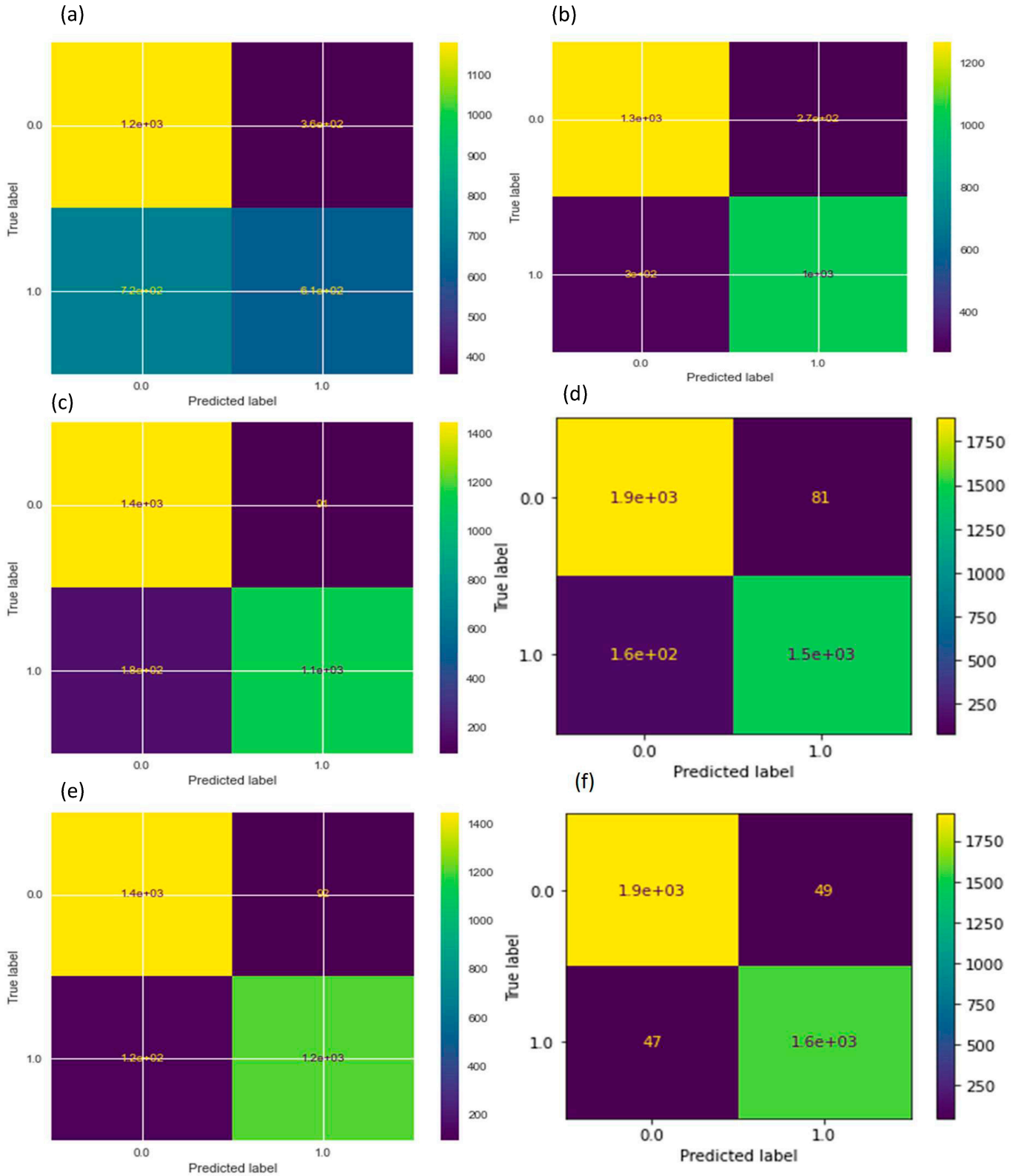

Figure 8. The proposed DSC-LightGBM system's confusion matrix to recognize stress and anxiety where figures (**a**–**f**) were calculated based on 8 m, 12 m, 16 m, 22 m, 25 m, and 30 m, respectively.

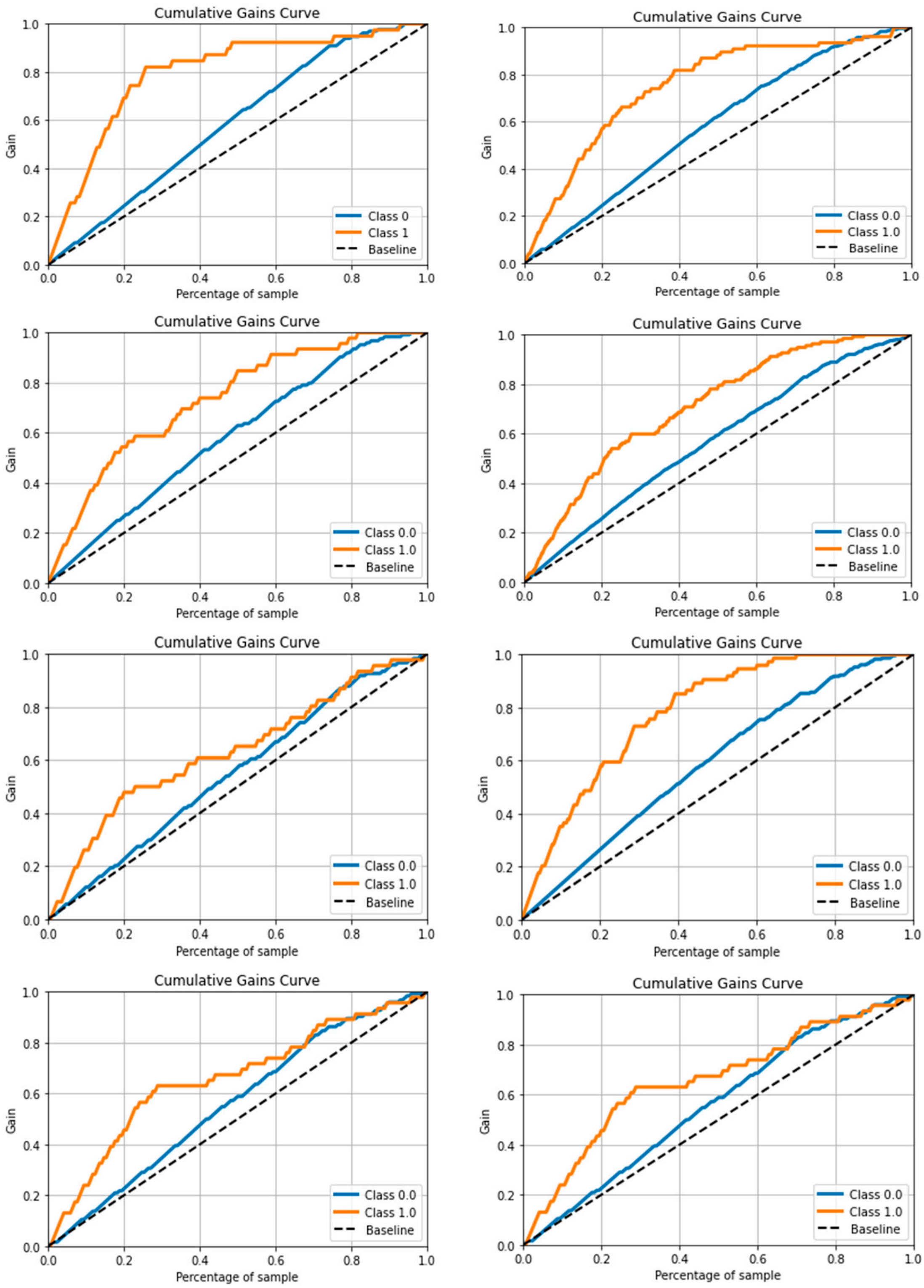

Figure 9. Results of proposed DSC-LightGBM model using area under curve (AUC) on post-COVID-19 EEG dataset based on epochs (50, 100, 150, 200, 250, 300, 350, 400); class 0 displays anxiety and class 1 represents stress emotion.

The proposed RCN-L model properly detected all the emotion classes utilized in the datasets, as shown by the confusion matrix used in Figure 8 with various test/validation/train ratios. The 15%/15%/70% ratio was used in Figure 8a. The 10%/10%/80% ratio was used in Figure 8b, and the 20%/20%/60% ratio was used in Figure 8c. In Figure 8d, the

25%/25%/50% ratio was used. The confusion matrices from Figure 8a–d were calculated by using 12 m recorded EEG signals. In Figure 8e, where the 20%/20%/60% ratio was used, and Figure 8f where the 20%/20%/60% ratio was used, 16 m of EEG signals were used. It was discovered that the projected label for every category did not become confused even when the model was trained on a limited dataset. Both categories were classified correctly. As can be seen from the confusion matrix, the suggested model RCN-L plus preprocessing stages had greater detection accuracy.

As shown in Table 6, the proposed approach RCN-L with LightGBM achieved excellent detection SE, SP, F1-score, and ACC. Using the proposed technique, the error rate on both datasets was extremely low. This paper was able to achieve 92 percent accuracy, precision, and recall using the DSC architecture and the LightGBM classifier. This section compared the performance and computational complexity of the proposed RCN-L approach to existing state-of-the-art algorithms. There was no previous system available that could be compared directly to the proposed RCN-L architecture for the classification of stress and anxiety in terms of post-COVID-19 symptoms. As a result, to achieve this task, various experiments were conducted to compare the suggested work in different ways and they compared the proposed strategy to existing alternatives as measured in Tables 7–9. In these tables, we compared standard machine learning (ML) and deep learning (DL) techniques. Compared to ML algorithms, the DL algorithms provided somewhat good classification results. Especially in Table 7, we compared different brain disorders such as stress and anxiety using non-COVID-19 [52] and post-COVID-19 patients. The results are described in Table 7. From this table, it is clear that our proposed RCN-L outperformed using both the post-COVID-19 and the non-COVID-19 datasets. The results were compared to those of other models that have been built for detecting stress and anxiety based on 12 m and 16 m EEG spectrogram datasets. The VGG model performs well in detecting the classification error rate in stress images compared to anxiety states. However, the anxiety graphics are somewhat difficult to recognize. As a result, this paper achieved lower SE, SP, and F1-score values on the 12 m EEG recording segment compared to the 16 m EEG recording segment dataset.

Table 6. On selective 12 m and 16 m recorded EEG datasets, the detection results of the proposed RCN-L architecture.

Database	SE	SP	F1-Score	Recall	Precision	ACC
12m EEG	0.91	0.94	0.92	94%	94%	92%
16m EEG	0.92	0.93	0.91	94%	94%	93%

SE: Sensitivity, SP: specificity, RL: recall, PR: precision, ACC: accuracy, m: minutes.

Table 7. On selective 32 m recorded EEG dataset, the proposed technique utilizing RCN-L architecture for determining non-COVID-19 and post-COVID-19 stages of brain disorder.

Stages	SE	SP	F1-Score	Recall	Precision	ACC
Normal	0.94	0.95	0.94	98%	95%	96%
Stress	0.98	0.96	0.95	95%	98%	97%
Anxiety	0.94	0.93	0.94	94%	95%	96%
non-COVID-19	0.95	0.94	0.93	94%	94%	96%
Normal	0.94	0.94	0.95	92%	96%	94%
Stress	0.93	0.92	0.94	93%	97%	93%
Anxiety	0.92	0.93	0.93	91%	95%	95%
post-COVID-19	0.92	0.93	0.91	94%	94%	93%

SE: Sensitivity, SP: specificity, RL: recall, PR: precision, ACC: accuracy, non-COVID-19 dataset [52].

Table 8. On selective 16 m recorded EEG dataset, the average results produced by several standard machine learning algorithms.

ML Methods	SE	SP	F1-Score	Recall	Precision	ACC
ANN	0.58	0.60	0.56	59%	58%	59%
SVM	0.61	0.60	0.58	56%	56%	56%
AdaBoost	0.67	0.63	0.60	58%	57%	58%
Naïve Bayes	0.65	0.62	0.64	61%	60%	61%
LDA	0.54	0.53	0.52	52%	52%	52%
PCA	0.55	0.56	0.53	54%	53%	54%

SE: Sensitivity, SP: specificity, RL: recall, PR: precision, ACC: accuracy, ANN: artificial neural network, SVM: support vector machine, AdaBoost: adaptive boosting, LDA: linear discriminate analysis, PCA: principal component analysis.

Table 9. On selective 16 m recorded EEG dataset, the average results produced by several standard deep learning algorithms.

DL Methods	SE	SP	F1-Score	Recall	Precision	ACC
CNN	0.68	0.69	0.67	70%	72%	70%
LSTM	0.71	0.70	0.70	71%	70%	71%
Autoencoder	0.67	0.65	0.65	65%	63%	65%
RBM	0.72	0.70	0.70	69%	67%	69%
RBF	0.70	0.72	0.68	72%	70%	72%
SAE	0.72	0.70	0.70	71%	68%	71%

SE: Sensitivity, SP: specificity, RL: recall, PR: precision, ACC: accuracy, CNN: convolutional neural network, LSTM: long-term short-term memory, RBM: random Boltzmann machine, RBF: radial basis function, SAE: stack-based autoencoder.

The Alex-Net performs well on the 16-m EEG recording dataset but not so well on the 12-m EEG recording dataset when it comes to detecting stress and anxiety. As a result, on 12 m and 16 m EEG recordings, the Alex-Net model produced lower SE, SP, AUC, and F1-score. The Alex-training Net's process is lengthy, and it takes more than 400 epochs to achieve satisfactory results. It was also discovered that the Xception Network's performance in the detection of anxiety in spectrogram images is somewhat lacking. On both 12 m and 16 m EEG datasets, it was discovered that the suggested technique performs well enough and outperforms the other models. Tables 10–12 show the results of an experiment using several detection methods to compare the proposed method to existing models using a 16 m EEG dataset. The MLP-CNN [33], BiLSTM [30], and InceptionResnetV2 [26] systems were selected to perform comparisons with the proposed RCN-L architecture using EEG spectrogram images. Compared to the other methods, the RCN-L outperformed in terms of SE, SP, ACC, and F1-score. This highlighted the capability of the suggested work for the recognition of stress and anxiety accurately when performed using spectrogram images. As shown in Table 13, the results demonstrated that the proposed strategy outperformed the existing deep learning models. All three measures showed that this method is effective. This paper concludes that the proposed method is suitable for identifying stress and anxiety using EEG spectrogram images.

Table 10. Using datasets with and without preprocessing procedures, comparison of the proposed strategy to existing work.

Method	SE	SP	F1-Score	ACC
MLP-CNN [33]	74%	74%	74%	0.72
	82%	87%	82%	0.81
BiLSTM [30]	76%	76%	71%	0.75
	80%	82%	81%	0.79
InceptionResnetV2 [26]	83%	89%	82%	0.81
	84%	86%	85%	0.82
CNN-TCN [34]	67%	67%	67%	0.65
	73%	79%	72%	0.73
Proposed Model	92%	92%	92%	0.92

SE: Sensitivity, SP: specificity, RL: recall, PR: precision, ACC: accuracy.

Table 11. Comparison of the proposed method to previous research.

Method	SE	SP	F1-Score	Accuracy
MLP-CNN [33]	88%	84%	86%	87%
BiLSTM [30]	86%	96%	91%	94%
InceptionResnetV2 [26]	83%	89%	82%	93%
Proposed Method	92%	92%	92%	92%

Table 12. Evaluation of the proposed method against existing work utilizing a variety of datasets from various research and other deep learning classifiers.

Method	SE	SP	F1-Score	ACC
MLP-CNN [33]	83%	81%	80%	81%
BiLSTM [30]	82%	84%	84%	84%
InceptionResnetV2 [26]	82%	97%	89%	88%
VGG-16	86%	96%	91%	94%
Alex-Net	90%	92%	91%	87%
Xception	83%	89%	82%	93%
Proposed	92%	92%	92%	92%

SE: Sensitivity, SP: specificity, ACC: accuracy.

Table 13. Average processing time on an EEG dataset with a recording period of 30 min.

Method	Preprocessing	Feature Extraction	Training	Prediction	Overall
MLP-CNN [33]	NA	2.0 s	180.2 s	1.8 s	184 s
BiLSTM[30]	NA	2.2 s	205.1 s	1.9 s	209.2 s
Proposed	1.6 ms	1.8 ms	160.5 ms	1.4 ms	164.5 ms

ms: milliseconds, s: seconds.

Gradient-weighted Class Activation Mapping (Grad-CAM) [53] images are shown in Figure 10 to demonstrate that the mid-level frequency components of stress, anxiety, and normal patients' EEG spectrograms exhibit particular patterns that allow the records to be distinguished. The approach described in this research may be applied as a foundation for CAD investigations that seek to identify specific brain disorders that are thought to leave some evidence in the EEG recordings.

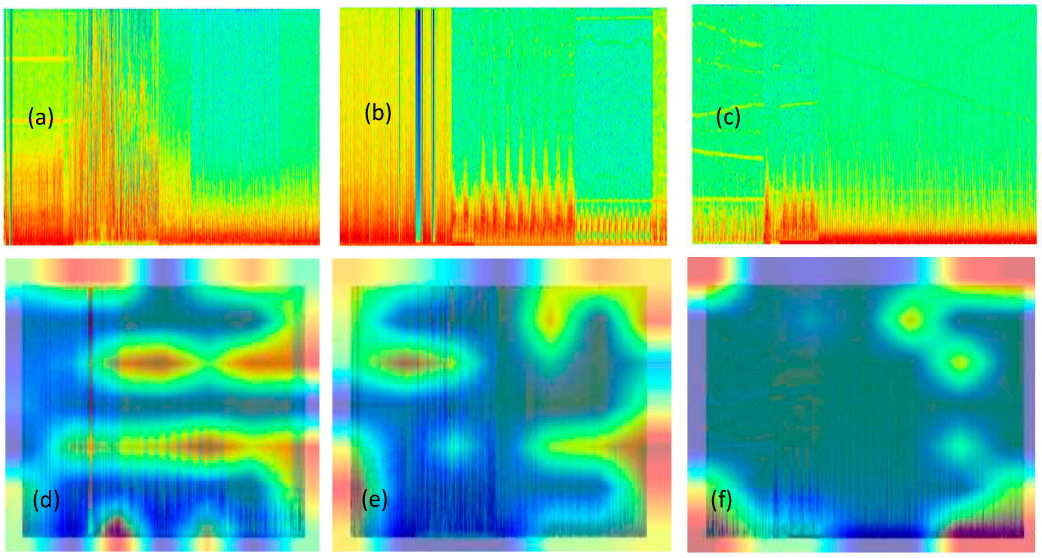

Figure 10. Results of proposed RCN-L model using Grad-CAM [53], where figures (**a**–**c**) show the anxiety, stress, and normal patterns of patients, respectively, and figures (**d**–**f**) represent the corresponding Grad-CAM results.

4.5. Gernalizability of Classifier

To test the generalizability of the proposed RCN-L technique, we compared the developed system on a non-COVID-19 [52] dataset with similar brain disorders. In [53], a mental disorder called a "psychiatric condition" is one that has been identified by a mental health expert. In this dataset, many different psychiatric illnesses have been presented. However, we have selected only stress, anxiety, and normal patients' EEG signals. Those EEG signals were first subjected [36] to a denoising technique to expose their features. A wavelet threshold denoising method was utilized as described in study [36]. According to that research, DL in EEG may be able to predict serious psychiatric diseases and offer a reliable system to predict these conditions. The proposed RCN-L model's results were measured in terms of F1-score and accuracy on our datasets for post-COVID-19 and non-COVID-19 [52], as shown in Figure 11. These results were calculated by using EEG signals and the stress, anxiety, and normal conditions of patients. The proposed RCN-L classifier was superior and had the generalizability to be used in any clinical setting for determining brain disorders.

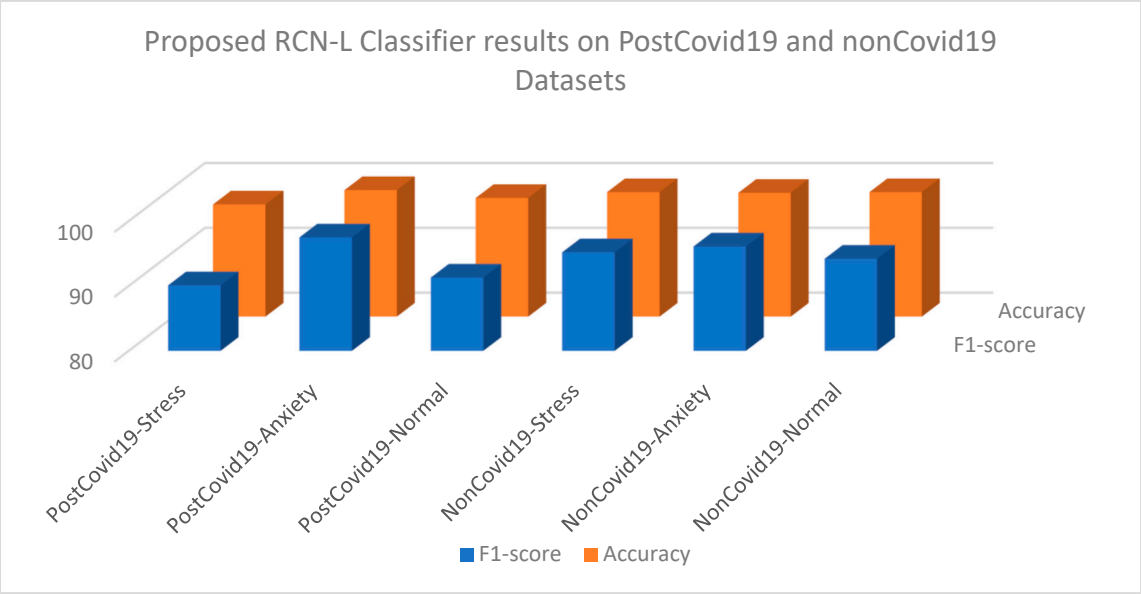

Figure 11. Results of proposed RCN-L model for F1-score and accuracy measures using post-COVID-19 and non-COVID-19 datasets [52]. These results were calculated by using EEG signals and stress, anxiety, and normal conditions of patients.

5. Discussion

The fundamental purpose of this research was to develop a new deep-learning (DL) model for detecting and classifying stress and anxiety in undergraduate students who have been infected with COVID-19. The diagnosis of these emotions using EEG signals effectively achieved the complexity challenge, confined the dataset, and extracted the feature in the existing DL architecture quickly. Furthermore, when compared to state-of-the-art CNN-based classification approaches, it achieved better classification accuracy. As indicated in the systematic diagram in Figure 1, the proposed RCN-L system has been developed based on four primary phases. In the first phase, the multi-channel EEG signals are preprocessed to remove artifacts, and these 1-D EEG signals are converted into a 2-D spectrogram image. In the second phase, the DS-Conv model with the residual network is utilized to extract relevant features. The unique DS-Conv-based classifier is then given these features, which creates probabilities for every output class in different time blocks. In the fourth phase, the LightGBM handling step integrates probabilities from several time blocks to boost detection confidence. To extract features from spectrogram images, the DSC and residual connection-based CNN models are used first. The images are then classified

using LightGBM classifier into stress and anxiety. The advantages of the suggested (RCN-L) approach for identifying and classifying stress and anxiety emotions using preprocessed spectrogram images have been discussed. To detect stress and anxiety feelings, it was decided to utilize CNN as a foundation system based on DSC with a light gradient boosting machine (LightGBM).

This paper collected datasets privately for the evaluation of the proposed work. First, it used the augmentation approach to enhance the data size. After that, this paper extracted features from spectrogram images using the first flow of the MobileNet model, which is based on depthwise–pointwise separable networks and residual connectivity. Finally, it used the feature map for the classification of the images into stress and anxiety spectrogram images using a LightGBM classifier. According to the results in Table 4, the complete dataset delivered the best accuracy (91.98 percent) when utilizing the LightGBM classifier for identifying features to classify the stress, anxiety, and non-stress status tasks (almost perfect agreement). There was a need to use the confusion matrix to fully measure the detection performance. The confusion matrices revealed that the expected and actual labels were not in concordance. The genuine label for each row was presented on the row labels, while the predicted label for every column was displayed on the column labels. The color indicated the proportion of records in the same row as the total number of records. Consequently, depending on the test set classified by the RCN-L model, this study was able to acquire the results of two categories, such as anxiety and stress.

As shown in Tables 6–13, the proposed approach RCN-L with LightGBM achieved excellent detection SE, SP, F1-score, and ACC. Using the proposed technique, the error rate on both datasets is extremely low. We were able to achieve 92 percent accuracy, precision, and recall using the DSC architecture and the LightGBM classifier. Similarly, the area under the curve (AUC) curve was also measured to show the performance of the proposed RCN-L model. Figure 8 represents the various AUC curves when measured for different sets of epochs (50, 100, 150, 200, 250, 300, 350, 400). On average, the 0.92 AUC measures how well people recognize stress and anxiety emotions. In this paper, various segments of EEG spectrogram images were used to assess the model's performance. The confusion matrix in Figure 6 shows that the proposed model correctly detects all the emotion classes used in datasets. It was discovered that the projected label for every category does not become confused even when the model is trained on a limited dataset. Both categories are classified correctly. As can be seen from the confusion matrix, the suggested model RCN-L, along with a preprocessing stage to remove artifacts, has a greater detection accuracy.

It is preferable to conduct the EEG experiment on all participants at the same time of day to avoid the effects of time on cognitive ability and the implications of circadian rhythm for stress performance. The task nature and sample size had a direct impact on classifier accuracy, such as the limited duration of mental arithmetic tasks, which leads to low-performance accuracy [43], and the mixed findings obtained with large numbers of participants in [24,42,43]. It is worth emphasizing that most of the research has a small sample size, which means that the number of people participating was not large enough to overcome preconceptions based on individual variations. Furthermore, in these experiments, the data augmentation technique was applied to increase the dataset size. Many studies have provoked stress in controlled situations, whereas developing a technique that can withstand real-world scenarios, such as virtual reality, is a superior method. Furthermore, the ground truth that is required to train the classifier by separating people into stress and anxiety groups is a significant aspect that determines stress assessment findings. Most of the research used a mathematical questionnaire, a psychological interview, or both, to determine this labeling. However, because of the heavy reliance on participants, these two methodologies were unable to provide a direct assessment of the presence of mental stress. Unlike in simulated tests, labeling subjects in real-world tasks is a considerable problem. This study is proposing EEG feature extraction techniques for increasing stress detection, such as phase synchronization and source localization, as future research.

Despite having a small dataset from our study and experiments, the post-COVID-19 EEG images were significantly different from the others in all statistical tests. There are several techniques for extracting features, including time series domain and frequency domain techniques, and new techniques are always being created. For ML or DL to conduct dimensional reduction and improve prediction accuracy, meaningful feature extraction is essential [46]. The current study employed coherence approach to extract robust features in case of noise from 2-D spectrogram images. Our findings can be used to provide diagnostic data and support tailored treatment decisions. The EEG using DL has shown encouraging results for predicting treatment responses. Additionally, compared to the paradigm involving experimental stimulation, the task-free and resting-state technique for EEG recording requires less measuring time, making it more accessible and scalable.

As a result, we discovered that, depending on the diagnosis, a DL technique employing EEG may accurately predict major mental diseases to varying degrees. Several EEG feature characteristics were illustrated in each condition categorization model. EEG-DL is a promising method for categorizing psychiatric diseases. It has the ability to support clinical judgments based on evidence and offer objectively quantifiable biomarkers. Future medical healthcare that uses BCI and automated diagnostic technologies might be useful.

The mental healthcare field is evolving quickly due to data and computational science breakthroughs. The range of data we can measure has increased with regard to neurological processes and objective indicators. Furthermore, the application of machine learning (ML), deep learning (DL), or artificial intelligence (AI), has grown. Out-of-sample estimates allow machine learning (ML) to prospectively evaluate the efficacy of predictions on new data (test data) that was not used for model fitting (training data), thereby producing results that may have a high level of clinical translation. This method differs from traditional inference based on null hypothesis tests (such as the *t*-test and analysis of variance), which retroactively concentrate on in-sample estimates and group differences and lack individualized explanation. ML is expected to supplement or even replace clinical judgments, such as diagnosis, prognosis, and treatment outcome prognosis.

The current study contains a few drawbacks. First, there was no control over the noise or muscular movements on the selected EEG signals. Second, diagnoses were made close to the time that EEGs were taken, so we cannot completely rule out the possibility of individuals having mixed findings who were later diagnosed with various diseases. Third, the sample comes from a single center and only in a certain environment. The model should be evaluated for different environments in terms of race and nationality. Finally, we did not prospectively validate the model because our methodology is retrospective. Moreover, no additional samples were received for external validation. As a result, more samples must be used to confirm the results before making any generalizations.

The experimental results show that classification accuracy for emotions is possible because we developed a lightweight pre-trained model with a computational efficiency solution which requires fewer parameters. When compared to other classifiers, our proposed RCN-L system outperforms them, which proves that the proposed model is unique compared to the state-of-the-art approaches.

6. Conclusions

Sensors embedded in physical devices, as well as machine learning methods, are used by IoT devices to monitor and exchange data. As the number of cases of post-COVID-19 rises rapidly, it is more important than ever to detect, diagnose, and control emotions early. In this study, the RCN-L model with preprocessing steps has been proposed as a stress-inducing protocol, and different aspects of EEG multichannel signals have been examined using time-series physiological data collected from 120 undergraduate students. EEG-based deep learning approaches to emotion detection are computationally demanding, limiting memory potency, training, and hyperparameter tuning. As a result, they are inappropriate for real-time applications with limited computational resources, such as the detection of post-COVID-19 anxiety and stress. The accuracy, precision, recall, F1-score, and AUC

of the suggested redundancy-reduced depthwise separable convolution network were 0.9163, 0.9246, 0.9282, 0.9264, and 0.9263, respectively. There were only 20,686 parameters employed in the proposed approach. The proposed network avoided the time-consuming detection and classification of emotions for post-COVID-19 while still achieving impressive network training performance and a significant reduction in learnable parameters. With the use of electroencephalography, we sought to create a machine-learning (ML) classifier that can identify and contrast the main mental diseases (EEG). In the past, we gathered information from medical records. Models for the categorization of individuals with each disease were established using a combination of factors at different frequency bands. This paper also concluded that emotions are impacted by post-COVID-19 scenarios. In the future, we will use this RCN-L model for post-COVID-19 patients to analyze employee performance.

Author Contributions: Conceptualization, Q.A., A.R.B. and A.H.; methodology, Q.A. and A.H.; software, Q.A.; validation, Q.A., A.R.B. and A.H.; resources, Q.A., A.H. and A.R.B.; data curation, Q.A. and A.H.; writing—original draft preparation, Q.A., A.R.B. and A.H.; writing—review and editing, Q.A.; visualization, Q.A. and A.R.B.; supervision, A.R.B.; funding acquisition, A.R.B. All authors have read and agreed to the published version of the manuscript.

Funding: The authors extend their appreciation to the Deanship of Scientific Research at Imam Mohammad Ibn Saud Islamic University (IMSIU) for funding and supporting this work through Research Partnership Program no. RP-21-07-04.

Institutional Review Board Statement: Not applicable.

Informed Consent Statement: Not applicable.

Data Availability Statement: The Post-COVID-19 dataset generated for this study is available on request to the corresponding author, whereas the non-COVID-19 dataset can be downloaded from the link: https://www.kaggle.com/datasets/shashwatwork/eeg-psychiatric-disorders-dataset (accessed on 7 November 2022).

Acknowledgments: The authors extend their appreciation to the Deanship of Scientific Research at Imam Mohammad Ibn Saud Islamic University (IMSIU) for funding and supporting this work through Research Partnership Program no. RP-21-07-04.

Conflicts of Interest: The authors declare no conflict of interest.

References

1. Gupta, A.; Jain, V.; Singh, A. Stacking Ensemble-Based Intelligent Machine Learning Model for Predicting Post-COVID-19 Complications. *New Gener. Comput.* **2021**, *40*, 987–1007. [CrossRef] [PubMed]
2. Cau, R.; Faa, G.; Nardi, V.; Balestrieri, A.; Puig, J.; Suri, J.S.; SanFilippo, R.; Saba, L. Long-COVID diagnosis: From diagnostic to advanced AI-driven models. *Eur. J. Radiol.* **2022**, *148*, 110164. [CrossRef] [PubMed]
3. Kumar, R.; Mukherjee, S.; Choi, T.-M.; Dhamotharan, L. Mining voices from self-expressed messages on social-media: Diagnostics of mental distress during COVID-19. *Decis. Support Syst.* **2022**, *162*, 113792. [CrossRef] [PubMed]
4. Jain, A.; Yadav, K.; Alharbi, H.F.; Tiwari, S. Iot & ai enabled three-phase secure and non-invasive COVID-19 diagnosis system. *Comput. Mater. Contin.* **2022**, *71*, 423–438.
5. Watson, C.J.; Thomas, R.H.; Solomon, T.; Michael, B.D.; Nicholson, T.R.; Pollak, T.A. COVID-19 and psychosis risk: Real or delusional concern? *Neurosci. Lett.* **2021**, *741*, 135491. [CrossRef]
6. Ardabili, S.; Mosavi, A.; Ghamisi, P.; Ferdinand, F.; Varkonyi-Koczy, A.; Reuter, U.; Rabczuk, T.; Atkinson, P. COVID-19 Outbreak Prediction with Machine Learning. *Algorithms* **2020**, *13*, 249. [CrossRef]
7. Rehman, I.U.; Sobnath, D.; Nasralla, M.M.; Winnett, M.; Anwar, A.; Asif, W.; Sherazi, H.H.R. Features of Mobile Apps for People with Autism in a Post COVID-19 Scenario: Current Status and Recommendations for Apps Using AI. *Diagnostics* **2021**, *11*, 1923. [CrossRef]
8. Khowaja, S.; Khuwaja, P.; Dev, K. Internet of everything enabled solution for COVID-19, its new variants and future pandemics: Framework, challenges, and research directions. *arXiv* **2021**, arXiv:2101.02030.
9. Rivera, M.J.; Teruel, M.A.; Maté, A.; Trujillo, J. Diagnosis and prognosis of mental disorders by means of EEG and deep learning: A systematic mapping study. *Artif. Intell. Rev.* **2022**, *55*, 1209–1251. [CrossRef]
10. Samee, N.; El-Kenawy, E.; Atteia, G.; Jamjoom, M.; Ibrahim, A.; Abdelhamid, A.A.; El-Attar, N.E.; Gaber, T.; Slowik, A.; Shams, M.Y. Metaheuristic optimization through deep learning classification of COVID-19 in chest X-ray images. *Comput. Mater. Contin.* **2022**, *73*, 4193–4210.

11. Xia, L.; Feng, Y.; Guo, Z.; Ding, J.; Li, Y.; Li, Y.; Ma, M.; Gan, G.; Xu, Y.; Luo, J.; et al. MuLHiTA: A Novel Multiclass Classification Framework With Multibranch LSTM and Hierarchical Temporal Attention for Early Detection of Mental Stress. *IEEE Trans. Neural Networks Learn. Syst.* **2022**, 1–14. [CrossRef] [PubMed]
12. Wang, Z.; Zhang, J.; He, Y.; Zhang, J. EEG emotion recognition using multichannel weighted multiscale permutation entropy. *Appl. Intell.* **2022**, *52*, 12064–12076. [CrossRef]
13. Jagadeeswari, V.; Vairavasundaram, S.; Logesh, R.; Vijayakumar, V. A study on medical Internet of Things and Big Data in personalized healthcare system. *Health Inf. Sci. Syst.* **2018**, *6*, 14. [CrossRef]
14. Cheng, B.; Fan, C.; Fu, H.; Huang, J.; Chen, H.; Luo, X. Measuring and Computing Cognitive Statuses of Construction Workers Based on Electroencephalogram: A Critical Review. *IEEE Trans. Comput. Soc. Syst.* **2022**, *9*, 1644–1659. [CrossRef]
15. Santhiya, P.; Chitrakala, S. PTCERE: Personality-trait mapping using cognitive-based emotion recognition from electroencephalogram signals. *Vis. Comput.* **2022**, *9*, 1–15. [CrossRef]
16. Gao, Q.; Wang, C.-H.; Wang, Z.; Song, X.-L.; Dong, E.-Z.; Song, Y. EEG based emotion recognition using fusion feature extraction method. *Multimed. Tools Appl.* **2020**, *79*, 27057–27074. [CrossRef]
17. Abbas, Q.; Qureshi, I.; Yan, J.; Shaheed, K. Machine Learning Methods for Diagnosis of Eye-Related Diseases: A Systematic Review Study Based on Ophthalmic Imaging Modalities. *Arch. Comput. Methods Eng.* **2022**, *29*, 3861–3918. [CrossRef]
18. Wang, Y.R.; Kanemura, A. Designing Lightweight Feature Descriptor Networks with Depthwise Separable Convolution. *Annu. Conf. Jpn. Soc. Artif. Intell.* **2021**, *1357*, 183–191. [CrossRef]
19. Shaheed, K.; Mao, A.; Qureshi, I.; Kumar, M.; Hussain, S.; Ullah, I.; Zhang, X. DS-CNN: A pre-trained Xception model based on depth-wise separable convolutional neural network for finger vein recognition. *Expert Syst. Appl.* **2022**, *191*, 116288. [CrossRef]
20. Shaheed, K.; Mao, A.; Qureshi, I.; Abbas, Q.; Kumar, M.; Zhang, X. Finger-vein presentation attack detection using depthwise sep-arable convolution neural network. *Expert Syst. Appl.* **2022**, *198*, 116786. [CrossRef]
21. Anbarasi, A.; Ravi, S.; Vaishnavi, J.; Matla, S.V.S.B. Computer aided decision support system for mitral valve diagnosis and classification using depthwise separable convolution neural network. *Multimed. Tools Appl.* **2021**, *80*, 21409–21424. [CrossRef]
22. Wei, Y.; Wu, Y.; Tudor, J. A real-time wearable emotion detection headband based on EEG measurement. *Sens. Actuators A Phys.* **2017**, *263*, 614–621. [CrossRef]
23. Sakalle, A.; Tomar, P.; Bhardwaj, H.; Acharya, D.; Bhardwaj, A. A LSTM based deep learning network for recognizing emotions using wireless brainwave driven system. *Expert Syst. Appl.* **2021**, *173*, 114516. [CrossRef]
24. Cui, H.; Liu, A.; Zhang, X.; Chen, X.; Wang, K.; Chen, X. EEG-based emotion recognition using an end-to-end regional-asymmetric convolutional neural network. *Knowl. Based Syst.* **2020**, *205*, 106243. [CrossRef]
25. Zhang, J.; Yin, Z.; Chen, P.; Nichele, S. Emotion recognition using multi-modal data and machine learning techniques: A tutorial and review. *Inf. Fusion* **2020**, *59*, 103–126. [CrossRef]
26. Cimtay, Y.; Ekmekcioglu, E.; Caglar-Ozhan, S. Cross-Subject Multimodal Emotion Recognition Based on Hybrid Fusion. *IEEE Access* **2020**, *8*, 168865–168878. [CrossRef]
27. Koelstra, S.; Muhl, C.; Soleymani, M.; Lee, J.-S.; Yazdani, A.; Ebrahimi, T.; Pun, T.; Nijholt, A.; Patras, I. DEAP: A Database for Emotion Analysis; Using Physiological Signals. *IEEE Trans. Affect. Comput.* **2011**, *3*, 18–31. [CrossRef]
28. Bazgir, O.; Mohammadi, Z.; Habibi, S. Emotion recognition with machine learning using EEG signals. In Proceedings of the IEEE 25th National and 3rd International Iranian Conference on Biomedical Engineering (ICBME), Qom, Iran, 29–30 November 2018; pp. 1–5.
29. Islam, R.; Moni, M.A.; Islam, M.; Mahfuz, R.A.; Islam, S.; Hasan, K.; Hossain, S.; Ahmad, M.; Uddin, S.; Azad, A.; et al. Emotion Recognition From EEG Signal Focusing on Deep Learning and Shallow Learning Techniques. *IEEE Access* **2021**, *9*, 94601–94624. [CrossRef]
30. Joshi, V.M.; Ghongade, R.B. EEG based emotion detection using fourth order spectral moment and deep learning. *Biomed. Signal Process. Control.* **2021**, *68*, 102755. [CrossRef]
31. Mokatren, L.S.; Ansari, R.; Cetin, A.E.; Leow, A.D.; Ajilore, O.A.; Klumpp, H.; Vural, F.T.Y. Eeg classification by factoring in sensor spatial config-uration. *IEEE Access* **2021**, *9*, 19053–19065. [CrossRef]
32. Demir, F.; Sobahi, N.; Siuly, S.; Sengur, A. Exploring Deep Learning Features for Automatic Classification of Human Emotion Using EEG Rhythms. *IEEE Sens. J.* **2021**, *21*, 14923–14930. [CrossRef]
33. Sarkar, A.; Singh, A.; Chakraborty, R. A deep learning-based comparative study to track mental depression from EEG data. *Neurosci. Inform.* **2022**, *2*, 100039. [CrossRef]
34. Hashempour, S.; Boostani, R.; Mohammadi, M.; Sanei, S. Continuous Scoring of Depression From EEG Signals via a Hybrid of Convolutional Neural Networks. *IEEE Trans. Neural Syst. Rehabil. Eng.* **2022**, *30*, 176–183. [CrossRef] [PubMed]
35. Valero, E.; Gordo, M.; Blasco, M. EEG-based multi-level stress classification with and without smoothing filter. *Biomed. Signal Process. Control.* **2021**, *69*, 102881. [CrossRef]
36. Mamun, M.; Al-Kadi, M.; Marufuzzaman, M. Effectiveness of Wavelet Denoising on Electroencephalogram Signals. *J. Appl. Res. Technol.* **2013**, *11*, 156–160. [CrossRef]
37. Baygin, M.; Dogan, S.; Tuncer, T.; Barua, P.D.; Faust, O.; Arunkumar, N.; Abdulhay, E.W.; Palmer, E.E.; Acharya, U.R. Automated ASD detection using hybrid deep lightweight features extracted from EEG signals. *Comput. Biol. Med.* **2021**, *134*, 104548. [CrossRef]

38. Loh, H.W.; Ooi, C.P.; Aydemir, E.; Tuncer, T.; Dogan, S.; Acharya, U.R. Decision support system for major depression detection using spectrogram and convolution neural network with EEG signals. *Expert Syst.* **2022**, *39*, e12773. [CrossRef]
39. Pusarla, A.; Singh, B.; Tripathi, C. Learning DenseNet features from EEG based spectrograms for subject independent emotion recognition. *Biomed. Signal Process. Control.* **2022**, *74*, 103485. [CrossRef]
40. Cha, J.; Gu, K.; Toh, G.; Park, J.; Na, J.; Moon, J.-H. Electroencephalographic alpha oscillation as first manifestation of brain res-toration after resuscitation. *Neurol. Sci.* **2022**, *43*, 4025–4028. [CrossRef]
41. Ali, O.; Saif-Ur-Rehman, M.; Dyck, S.; Glasmachers, T.; Iossifidis, I.; Klaes, C. Enhancing the decoding accuracy of EEG signals by the introduction of anchored-STFT and adversarial data augmentation method. *Sci. Rep.* **2022**, *12*, 4245. [CrossRef]
42. Al-Saegh, A.; Dawwd, S.A.; Abdul-Jabbar, J.M. Deep learning for motor imagery EEG-based classification: A review. *Biomed. Signal Process. Control.* **2021**, *63*, 102172. [CrossRef]
43. Abdou, A.A. Literature review: Efficient deep neural networks techniques for medical image analysis. *Neural Comput. Appl.* **2022**, *34*, 5791–5812. [CrossRef]
44. Zargar, B.S.; Mollaei, M.R.K.; Ebrahimi, F.; Rasekhi, J. Generalizable epileptic seizures prediction based on deep transfer learning. *Cogn. Neurodynamics* **2022**, 1–13. [CrossRef]
45. Ma, Y.; Zhao, R.; Yan, K.; Liu, E. A real-time embedded drogue detection method based on lightweight convolution neural network for autonomous aerial refueling. *Neural Comput. Appl.* **2022**, *34*, 13425–13437. [CrossRef]
46. Ibrahem, H.; Salem, A.; Kang, H.-S. DTS-Net: Depth-to-Space Networks for Fast and Accurate Semantic Object Segmentation. *Sensors* **2022**, *22*, 337. [CrossRef] [PubMed]
47. Li, Y.; Yang, D.; Chen, Y.; Peng, C.; Sun, Z.; Jiao, L. A Lightweight Top-Down Multi-Person Pose Estimation Method Based on Symmetric Transformation and Global Matching. *IEEE Access* **2022**, *10*, 22112–22122. [CrossRef]
48. Wu, L.; Cai, N.; Liu, Z.; Yuan, A.; Wang, H. A one-stage deep learning framework for automatic detection of safety harnesses in high-altitude operations. *Signal Image Video Process.* **2022**, 1–8. [CrossRef]
49. Qiu, Y.; Ding, S.; Yao, N.; Gu, D.; Li, X. HFS-LightGBM: A machine learning model based on hybrid feature selection for classifying ICU patient readmissions. *Expert Syst.* **2021**, *38*, e12658. [CrossRef]
50. Wang, D.-N.; Li, L.; Zhao, D. Corporate finance risk prediction based on LightGBM. *Inf. Sci.* **2022**, *602*, 259–268. [CrossRef]
51. Cheng, W.; Li, J.; Xiao, H.; Ji, L. Combination predicting model of traffic congestion index in weekdays based on LightGBM-GRU. *Sci. Rep.* **2022**, *12*, 2912. [CrossRef] [PubMed]
52. Park, S.M.; Jeong, B.; Oh, D.Y.; Choi, C.H.; Jung, H.Y.; Lee, J.-Y.; Lee, D.; Choi, J.-S. Identification of Major Psychiatric Disorders From Resting-State Electro-encephalography Using a Machine Learning Approach. *Front. Psychiatry* **2021**, *1398*, 1–12.
53. Chattopadhyay, A.; Sarkar, A.; Howlader, P.; Balasubramanian, V.N. Grad-CAM: Improved visual explanations for deep convolutional networks. *arXiv* **2017**, arXiv:1710.11063.